Motility of Chlamydomonas reinhardtii at different temperatures

Author:
Yikai Zhao

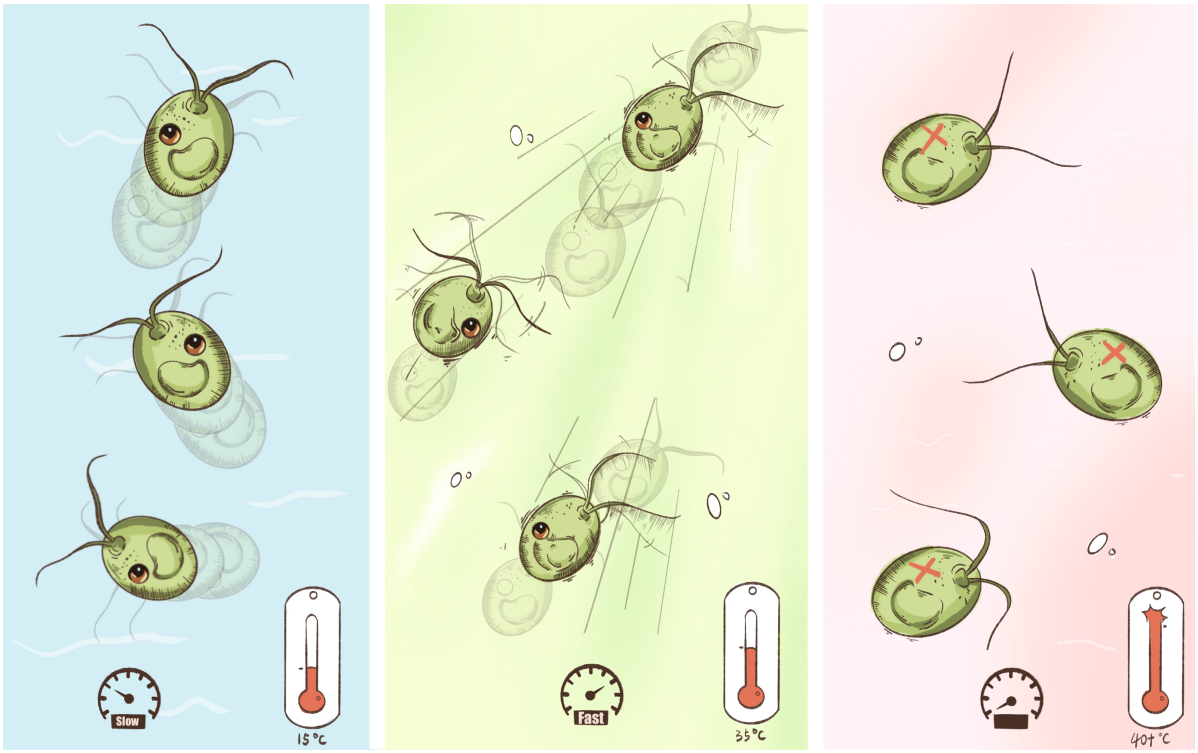

Mechanical Engineering
Process & Energy department
EFPT (Energy, Flow, Process technology) track

Supervisor: Dr. D.S.W. Tam
Daily supervisor: Sowmya Kumar

TU Delft

Motility of Chlamydomonas reinhardtii at different temperatures

The universe in a droplet

by

Yikai Zhao

to obtain the degree of **Master of Science**
in Mechanical Engineering
at the **Delft University of Technology**,
to be defended publicly on Friday 25th of August, 2023.

Student number: 5455251
Project duration: December, 2022 – August, 2023
Thesis committee: Dr. D.S.W. Tam, TU Delft
Dr. H.B. Eral, TU Delft
Sowmya Kumar, TU Delft

TU Delft

Preface

I am deeply grateful to my thesis supervisor, Dr.Daniel Tam, for your unwavering guidance, insightful feedback, and continuous encouragement throughout this research journey. Your vivid examples from the fluid dynamics class, such as the tea leaf paradox and climbing wine tears, brought this topic closer to our daily lives. During my master's thesis, you served not only as a supervisor but also as a mentor, helping me understand problems from perspectives I had never considered before.

I extend my gratitude to the instructors and professors who significantly shaped my academic journey during my two-year study at TUDelft. A special acknowledgment goes to Dr. Burak Eral, who took on the role of being a part of my thesis committee.

As my daily supervisor, Sowmya, your openness to answering even seemingly insignificant questions demonstrated your patience and professionalism. Your support greatly contributed to my thesis research's smooth and successful progress. Bob, your expert experimental advice was invaluable in helping me navigate challenges and avoid potential pitfalls. I would also like to extend my gratitude to Junaid and Koen for their remarkable work on the tracking code, which significantly influenced my research results. Being part of this research group, I feel fortunate to be surrounded by individuals who embrace challenges and readily offer assistance.

Furthermore, I want to express my gratitude to all the friends in my track who supported me and stood by me during the challenging times. Hamza, Ning, and Thomas, your friendly nature and willingness to help have been invaluable.

Lastly, my heartfelt thanks go to my family, especially my mother. Your unwavering emotional support played a pivotal role in enabling me to successfully complete my master's journey. I am reminded of Bruce Lee's wise words: 'Be like water, my friend.' This philosophy beautifully resonates with your teachings on navigating life's challenges and has guided me in becoming a better person.

– Yikai Zhao
Delft, August 2023

"Be like water making its way through cracks. Do not be assertive, but adjust to the object, and you shall find a way around or through it. If nothing within you stays rigid, outward things will disclose themselves. Empty your mind, be formless, shapeless, like water. If you put water into a cup, it becomes the cup. You put water into a bottle and it becomes the bottle. You put it in a teapot, it becomes the teapot. Now, water can flow or it can crash. Be water, my friend."

– Bruce Lee

Contents

List of Figures

Abstract

Algae remains a focal point of scientific inquiry with its wide-ranging environmental, health, and energy applications. Among model organisms, the unicellular green alga Chlamydomonas reinhardtii holds significance, particularly in light of its responsiveness to temperature alterations impacting swimming velocity. Notably, this study investigates the intriguing ability of live Chlamydomonas cells to modulate suspension viscosity compared to non-living particles.

Under shear flow conditions, a captivating phenomenon termed ”heat thickening” is unveiled in live algae suspensions. Unlike conventional fluids, heightened temperatures uniquely enhance viscosity in these suspensions due to the interplay between cell-generated stresslets and shear flow. This study aims to characterize the influence of temperature on microalgal swimming speeds, flagella beating frequencies, and its role in viscosity modulation.

An experimental setup with precise temperature control and water circulation is employed to achieve this. Both 2D and 3D tracking methods measure motility and inform the findings. Results demonstrate that swimming velocity and beating frequency increase with temperature until 35 degrees Celsius, followed by a decline. This trend aligns with the observed live cell suspension viscosity measurements, indicating the impact of motility on suspension rheology.

Quantitative research has indicated the simultaneous influence of beating frequency and swimming velocity on suspension viscosity, underscoring the importance of investigating motility’s role. This study suggests that the motility of live algae cells holds the potential for interpreting and modulating suspension rheology, warranting further exploration under various temperature conditions. Such insights contribute to understanding algae behavior and its applications across environmental and industrial contexts.

Keywords: *Chlamydomonas reinhardtii, Active fluid, Microalgal motility, Heat thickening, Temperature influence, Rheological properties*

1

Motivation

1.1. Microorganisms in our life

Any untreated drop of water from a lake, river, or ocean is a small world. It contains thousands of microscopic organisms, including bacteria, and algae. Algae and our daily lives are closely related. Algae is involved in various areas, including environmental issues, health treatments, and new energy technologies [33].

Nostoc is a filamentous cyanobacterial genus that has the ability to create macroscopic or microscopic colonies, and is widely distributed in both terrestrial and aquatic habitats [5]. According to historical records, the first recorded use of microalgae took place in China, when discovered that *Nostoc* was edible and nutritious, and began collecting it as a food source during a period of severe food shortages. *Nostoc* was particularly important because it could grow in environments where other crops could not, such as arid and rocky regions [7]. Since then, other cultures worldwide have also used microalgae as a food source. For example, the Aztecs and other Mesoamerican cultures used spirulina, blue-green algae, as a food source [1, 27]. Overall, using microalgae as a food source dates back thousands of years and has played an essential role in human survival and nutrition in various cultures throughout history [33]. In modern times, microalgae such as Chlorella and Dunaliella are also used as food supplements due to their high nutritional content [29]. However, interest in more expansive industrial production of microalgal biotechnology has only gained momentum since the middle of the 20th century. Nowadays, microalgae are extensively used in diverse commercial applications, including but not limited to, human and animal nutrition, biofuel production, cosmetics, production of high-value bioactive molecules, and pigments [33]. Viewed from a research perspective in section 1.2, exploring the interplay between fluid dynamics and microalgae represents a crucial field of investigation with wide-ranging implications.

Understanding the two-way interactions between algae and flow is not only relevant to industrial application but is also related to critical environmental questions. The investigation of algae is a subject of importance due to its strong association with various aspects of human development. Algae bloom refers the rapid proliferation or accumulation of algae

in freshwater or marine water systems, which can arise from the proliferation of both toxic and non-toxic algae. While algae bloom is a natural occurrence, it is of concern due to its negative impacts on aquatic species. For instance, a large number of aerobic algae may consume the oxygen in the water, leading to a decrease in oxygen levels for other aquatic species, ultimately affecting their survival. Therefore, the term ”Harmful Algal Bloom” (HAB) refers to the phenomenon that algae bloom harms other marine species [10]. Mitigating ”harmful algal blooms” (HAB) negative impact on marine life requires a thorough investigation of algae accumulation and motility. The presence of algae has long been associated with environmental concerns, particularly the emergence of harmful algal blooms (HABs). The role of flow in forming such blooms cannot be overlooked. Microbial communities have been shown to exhibit distinct behaviors in response to a range of environmental conditions, including the capacity of many microorganisms to migrate toward environments that facilitate their growth while avoiding unfavorable temperatures [30]. From this perspective, it is evident that investigations into the accumulation and motility of algae in fluid dynamics are critically linked to addressing environmental crises. Consequently, research on the motility of algae is not only unavoidable but also indispensable.

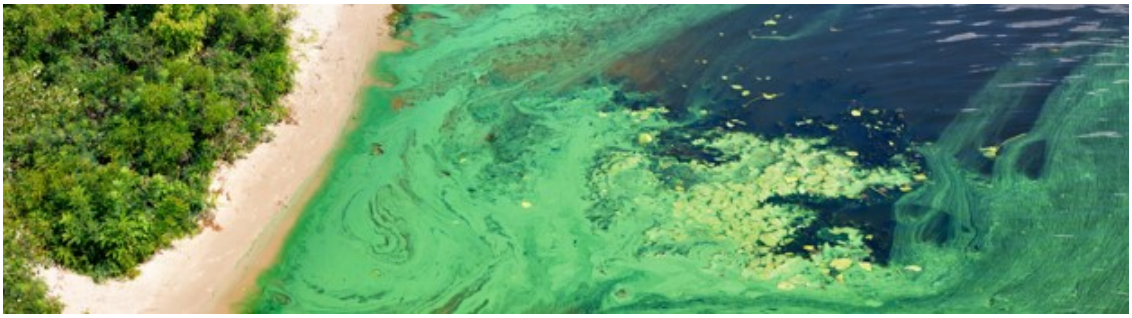

Figure 1.1: Harmful Algal Bloom. Source: Hallegraeff [10].

1.2. Algae Research

A range of physical and chemical factors, including pH, light, flow conditions, and temperature can influence the movements of microorganisms [30].

As a model organism, *Chlamydomonas reinhardtii*, a unicellular green alga, has been extensively studied over the past few decades [8]. Toshikazu’s research has found that temperature alterations can notably impact the swimming velocity of Chlamydomonas [19]. A previous study revealed that Chlamydomonas live cells contribute to a more pronounced augmentation of the suspension’s viscosity in comparison to dead algae. This outcome serves as evidence indicating that live algae cells can modulate the rheological properties of the suspension, particularly with regard to viscosity [26].

Nevertheless, despite these observed influences, the motility of *Chlamydomonas reinhardtii* under distinct temperature regimes and the precise mechanisms through which live algae cells modulate the rheological properties remain inadequately understood.

2

Active fluid & Rheology

2.1. Kinematics of live algae

An active fluid is composed of a collection of particles, cells, or macromolecules that possess the ability to convert chemical energy into mechanical work. These active agents are usually suspended in a viscous fluid [28]. Microalgae suspension is considered a type of active fluid. When measuring microalgae motility, it is necessary to consider several aspects of the experiment specific to this type of active fluid.

Figure 2.1: Bioreactors contains with live algae cells. Source: Aerin Einstein-Curtis [22].

2.1.1. Chlamydomonas reinhardtii & Motility

The wild-type *C. reinhardtii* cell has a wall made primarily of hydroxyproline-rich glycoproteins that resemble plant extensions and an average diameter of about 10 μm [8]. Its ease of cultivation and the possibility of genetic manipulation make it a biological model organism that is particularly well studied. Pulling by the two anterior flagella, *C. reinhardtii* cells are able to swim at an average speed of 100 μm/s. *C. reinhardtii* is typically grown in

a heterotrophic environment with white light illumination. In our experiments, we used the CC125 wild-type strain, which exhibits faster growth in light conditions compared to dark conditions. The optimal growth temperature is from 20° to 25° [11].

Motility can be a significant adaptation for heterotrophic bacteria and algae, and it can have implications for the ecology and biogeochemistry of the environment [9]. In this research, the motility of *C. reinhardtii* is evaluated through several parameters. Mean and median velocity calculations are the most common ways to interpret motility. Additionally, flagella beating frequency is a relevant measurement because of the movement of *C. reinhardtii* is generated by its flagella. Algae cells' turning angle and frequency is also important to investigate since they usually do not swim in a straight line.

2.1.2. Brownian motion

Given the small size of *C. reinhardtii* cells, it is natural to question whether Brownian motion might influence their movements. Brownian motion was first observed by botanist Robert Brown in 1828, who noticed the erratic motion of suspended pollen in water. This phenomenon, known as Brownian movement, is a well-established concept in physics, attributed to the random motion of water molecules continuously colliding with the pollen, causing its diffusion or dispersion in the water [15]. We introduce the Péclet number to characterize the effect of Brownian motion on cell motility, Péclet number is introduced as follows:

$$\mathrm{Pe} = \frac{\text{Advective transport rate}}{\text{Diffusive transport rate}} = \frac{Ua}{D} \tag{2.1}$$

Where U is the live cell swimming velocity (10^{-4}), a is the radius of *C. reinhardtii* (10^{-6}), D is the Stokes–Einstein equation expressed in $\frac{k_b T}{6\pi\eta a}$. k_b is the Boltzmann constant (10^{-23}), η is the dynamic viscosity of water (10^{-3}), T is the temperature in Kelvin (10^{2}).

$$\mathrm{Pe} = \frac{6\pi\eta U a^2}{k_b T} \approx 10^3 \tag{2.2}$$

Eq(2.2) indicates that the rate of molecular water diffusion is significantly lower than the rate of advective transport by the cells. The limitation of this result stems from the non-uniform swimming velocity and radius of the algae cells, but with the distribution values not exceeding three times. Consequently, Brownian motion can be disregarded in our research due to its minor impact.

2.1.3. Reynolds number & Kinematics

The Reynolds number (Re) is a dimensionless parameter commonly used to determine whether a fluid flow is turbulent or laminar. It is defined as the ratio between inertial force and viscous force. ($Re = \frac{\text{Inertial force}}{\text{Viscous force}}$). Eq(2.3) provides the mathematical formula for the Reynolds number (Re), which is dependent on the swimming velocity (U), characteristic length (D), and kinematic viscosity of the fluid (ν). For *C. reinhardtii*, the characteristic length is 10^{-5}m and the velocity scale is 10^{-4}m/s. Dimensional analysis reveals an extremely low Re number (10^{-3} at room temperature 25°C) due to the dominance of viscous forces in the

flow. At low Reynolds numbers, the flow is typically laminar, with viscous forces being the dominant forces in the system.

$$Re = \frac{U \cdot D}{\nu} \tag{2.3}$$

The motion of viscous fluids is typically described by the Navier-Stokes equations, which are a set of partial differential equations. In Einstein notation, the Navier-Stokes equations can be written as follows:

$$\frac{\partial \rho}{\partial t} + \frac{\partial (\rho u_i)}{\partial x_i} = 0 \tag{2.4}$$

$$\frac{\partial (\rho u_i)}{\partial t} + \frac{\partial (\rho u_i u_j)}{\partial x_j} = -\frac{\partial p}{\partial x_i} + \frac{\partial \tau_{ij}}{\partial x_j} + \rho f_i \tag{2.5}$$

The equations used in the experiment simplify the Navier-Stokes equations, which describe the motion of viscous fluids. Eq(2.4) represents the continuity equation, which assumes the conservation of mass. Eq(2.5) represents the conservation of momentum, known as the Cauchy momentum equation. The conditions of the experiment include the use of incompressible fluid, dominance of viscous forces, and a very low Reynolds number. These conditions allow for further simplification of the equations presented:

$$\rho \frac{\partial u_i}{\partial x_i} = 0 \tag{2.6}$$

$$0 = -\frac{\partial p}{\partial x_i} + \mu \frac{\partial^2 u_i}{\partial x_j^2} \tag{2.7}$$

Therefore, in the simplified momentum equation(2.7), the pressure and viscous terms remain while other terms, such as the convective acceleration term, are neglected due to the low Reynolds number.

2.2. Rheology of active fluid

Earlier studies have revealed that the swimming velocity of live algae cells can significantly influence the effective viscosity of the surrounding medium. This influence arises from the fact that self-propelled particles, such as live algae cells, exert forces on the surrounding medium as they move [26]. In our group research, we observed that temperature variations significantly impact the viscosity of the live suspension. Based on the findings of this research, one can deduce that temperature exerts a substantial impact on the viscosity of living microalgae suspensions, and there is a possibility that the motility of microalgae could affect the suspension's viscosity. Thus, exploring the effects of temperature variations on algae motility assumes great significance. Such knowledge is essential for effectively modulating algae behaviors in response to varying temperature conditions, facilitating enhanced industrial production performance while mitigating potential environmental concerns. Therefore, it is relevant to introduce the field of rheology and its pertinent aspects related to microalgae motility.

Rheology is the combination of two Greek words "$\rho\epsilon\omega$ (flow)" and "$-\lambda o\gamma\iota\alpha$ (study of)". It is the science of studying the deformation and flow of materials. To describe flow processes, constitutive relations establish a connection between stresses experienced within the medium and the resulting deformation and rate of deformation [37].

2.2.1. Newtonian & non-Newtonian fluid

Most low-molecular-weight substances show Newtonian flow properties, including molten metals and salts, organic and inorganic liquids, solutions of low-molecular-weight inorganic salts, and gases. The Newtonian fluid is characterized by a shear stress tensor (σ) that linearly depends on the rate of the shear tensor ($\dot{\gamma}$), and the proportionality constant is the well-known dynamic viscosity (η) [4]. Even though the concepts of flow and viscosity precede Newton, these fluids are traditionally referred to be Newtonian fluids [38]. A non-Newtonian fluid is characterized by the property that the stress is not necessarily proportional to the rate of the strain tensor. In other words, the relationship between stress and strain rate is not linearly dependent on the non-Newtonian fluids. Figure(2.2) shows the relation between shear stress and shear rate for Newtonian and non-Newtonian fluids.

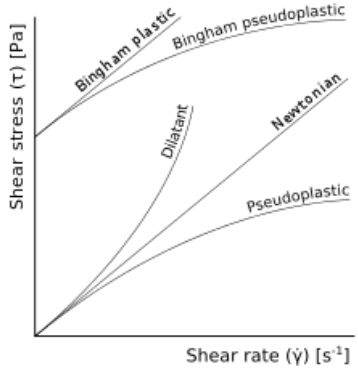

Figure 2.2: Shear stress (σ) vs. shear rate ($\dot{\gamma}$) plot. Source: Wikipedia [40].

Shear-thinning and shear-thickening are examples of non-Newtonian fluids, a fluid whose

viscosity is not constant but changes in response to the applied stress or strain rate. By evaluating the motility of microalgae, it becomes feasible to elucidate the theological measurement outcomes obtained in previous research, wherein it was observed that the viscosity of the live suspension exhibited substantial variations under distinct temperature conditions.

2.2.2. Puller & Pusher cells

According to the direction of fluid flow along the axis of net swimming, the flow fields produced by microswimmers are often categorized as either pusher or puller type [6, 17, 32]. A pusher swimmer propels itself forward by pushing the fluid backward with its flagella. In contrast, a puller swimmer uses a breaststroke-like swimming style to paddle the water from the front to the back, propelling itself forward. The interaction between different bacterial and algal populations forming microswimmers holds paramount importance in natural biological habitats and situations that necessitate medical and environmental remediation applications [31]. Consequently, research focusing on the motility of puller cells constitutes a significant aspect contributing to advancements in medical and environmental applications.

In the context of the active hydrodynamic contribution to rheology in a uniform forced shear flow, there is a fundamental difference in the mechanism between a pusher or a puller and a passive rodlike particle. While a pusher or puller can actively generate fluid flow, a passive rodlike particle lacks this ability and only responds to the external shear flow [12]. In the vicinity of the translating sphere, the shear flow can be decomposed into two distinct components: the rotating flow and the straining flow, which are added together to form the overall shear flow 2.3. The subsequent discussion will elucidate the impact of microorganism cells on a shear flow.

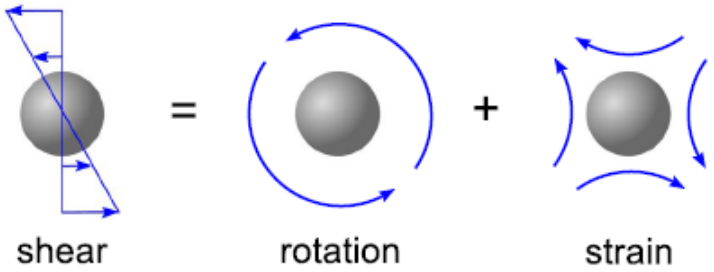

Figure 2.3: The flow of shear in the vicinity of a translating sphere can be characterized as a combination of straining and rotating flows. Source: Takagi [35].

The underlying mechanism responsible for the behavior of *C. reinhardtii* suspensions is not yet fully understood. However, a current rheological theory has been proposed to explain the modulation of viscosity resulting from cell motility which will be discussed in Section 2.2.4. The observation that puller cells also exhibit ”heat thickening” suggests that it may have implications for research on algae accumulation under shear flow conditions. Investigating this topic further could yield insights into how to prevent or mitigate the clogging or accumulation of algae in practical applications. Therefore, it remains a valuable area of research for the future.

2.2.3. Previous rheological research

According to previous rheological research, the viscosity in bacterial suspensions decreases as the volume fraction of particles increases. This counter-intuitive behavior can be attributed to the self-propelling nature of the particles, suggesting that their motility plays a crucial role [18]. In contrast, live Chlamydomonas cells significantly increase the viscosity of the suspension in comparison to deceased algae. This finding supports the notion that the presence of motility in live suspensions has a pronounced impact on their rheological properties [26].

Under shear flow conditions, our group's previous research has revealed an intriguing phenomenon in live algae suspensions referred to as "heat thickening." Typically, in common fluids, an increase in temperature leads to a decrease in viscosity. However, when we specifically increased the temperature of a live algae cell suspension with a cell density at 10^{13} cell/m^3, we observed an unexpected increase in viscosity, as illustrated in Figure 2.4. By comparing the magnitude of viscosity change between dead cell and live cell suspensions, we observed that the viscosity of live cell suspensions undergoes significant differences at different temperatures. In contrast, the viscosity of dead cell suspensions remains relatively unchanged with temperature variations. This observation contradicts conventional expectations and highlights the unique rheological behavior of live algae suspensions.

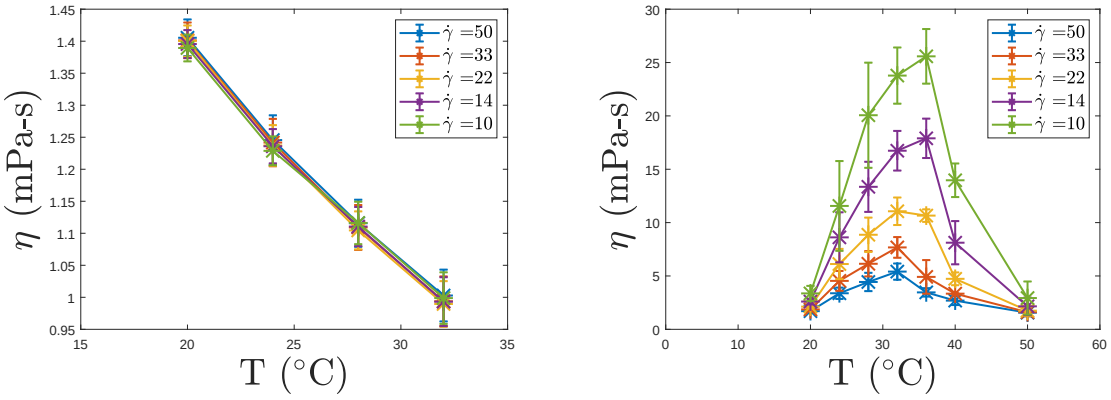

(a) Dead algae cell suspension viscosity in different temperatures and shear rate

(b) Live algae cell suspension viscosity in different temperatures and shear rate

Figure 2.4: The viscosity change of live and dead algae cell suspension. (a) Dead cell viscosity decrease when temperature increase, and the order of magnitude is between 1-1.4 mPa·s. (b) Live cell viscosity increase when temperature increase from 20 to 35 degrees Celsius, and the order of magnitude is between 1-25 mPa·s. Source: Sowmya Kumar. Rheological measurement in our lab.

Based on these findings, we can deduce that the motility of cells plays a significant role in modifying the rheological properties, particularly viscosity. This is supported by the observation that the most notable difference between live and dead cells is the presence of movement in live cells. The active motion and motility of live cells introduce additional complexity and interactions within the suspension, leading to significant changes in viscosity compared to dead cells.

2.2.4. Rheological theory

The rheological theory suggests that the presence of a cell can change viscosity in a shear flow through the generation of a stresslet. In particular, pusher cells generate a stresslet that its direction aligns with the pure straining motion in the shear flow, while puller cells produce a stresslet in the opposite direction. Based on Batchelor's illustration (figure2.5 (a)), the streamlines in the plane perpendicular to the z-axis (The z-axis is oriented perpendicular to the plane of the paper) exhibit a specific pattern for a stresslet configuration where the principal axes of the stresslet created by the particle align with the shear flow stresslet coordinate axes. In this case, elliptical-shaped passive particles demonstrate a symmetrical distribution of particle stress when subjected to an applied couple [2]. In the current scenario, the stresslet generated by the puller cells within a shear flow tends to oppose the direction of the shear flow stresslet, leading to a increase in the viscosity of the suspension.

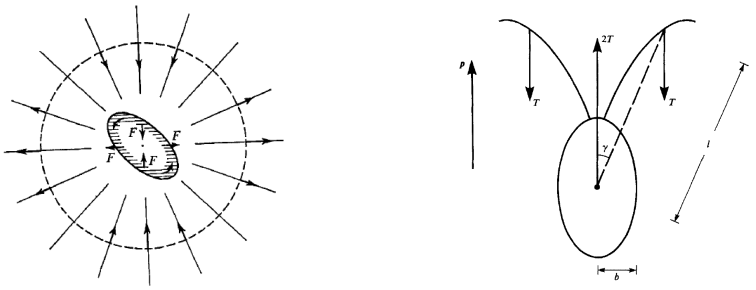

(a) Streamlines in the plane normal to the z-axis for a stresslet around a ellipsoid

(b) Schematic diagram of a swimming biflagellate

Figure 2.5: Flow field around passive ellipsoid and puller cell swimming diagram. (a) the ellipse represents the position of an ellipsoid undergoing rotational motion around the plane perpendicular to the z-axis. This rotation is induced by an applied couple, resulting in a symmetrical distribution of particle stresses. (b) illustrates the calculation of puller cell stresslet strength. Source: Batchelor [2], Pedley [25].

To provide a clearer illustration of the aforementioned concept, Figure2.6 shows a superposition of a pure straining motion in a shear flow and stresslet created by a passive particle and a cell. The overall effect of the puller cells leads to a decreased stresslet strength in a shear flow and an overall increase in the viscosity of the suspension. As the temperature of the suspension increases, the strength of the stresslet created by the puller cell also increases. This can be attributed to the enhanced motility of the cells at relatively higher temperatures. The increased temperature promotes more vigorous movement and activity of the cells, generating a stronger stresslet. Subsequently, the impact can be more extensively mitigated through the stresslet induced by shear flow.

In figure 2.5 (b), the symbol $\mathbf{p}$ denotes the cell orientation vector. The symbol $\boldsymbol{T}$ represents the thrust force exerted by the cell. The displacements of the points where the thrust forces are applied, relative to the center of the cell body, have a magnitude l and are inclined at an average angle γ.

$$S_{11} = -S_{22} = -2aF,\ S_{33} = 0 \tag{2.8}$$

Consider the biflagellate organism depicted in figure 2.5(b), where each flagellum exerts

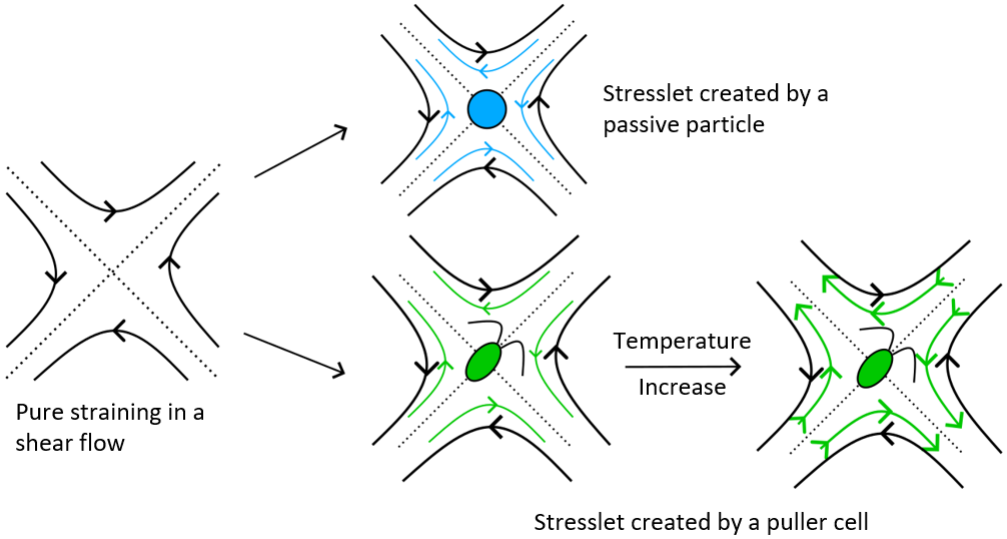

Figure 2.6: Schematic of the stresslet for a passive particle and live algae cell in straining motion.

an average thrust force -$T\mathbf{p}$ on the surrounding fluid, while the body of the organism exerts a drag force +$2T\mathbf{p}$. In the case of a spheroid-shaped organism moving with a relative speed V_s parallel to its axis, this force configuration is applicable [25]. Equation 2.9 illustrates that the thrust force (T) is dependent on various factors, including the dimensions (b) and eccentricity ($\alpha_F \approx 1.08$) of the cell body, the viscosity of the fluid (μ), and the mean swimming speed of the cell (V_s).

$$2T = 6\pi b\mu V_s \alpha_F \tag{2.9}$$

When neglecting inertia, the velocity field at a displacement x from the body, where x is much larger than the characteristic length scale l, is primarily influenced by the stresslet term [2]. The stresslet strength $\boldsymbol{S}$ is given by:

$$\boldsymbol{S} = 2Tl\cos\gamma(\mathbf{pp} - \frac{1}{3}\mathbf{I}) \tag{2.10}$$

According to equation 2.10, the strength of the stresslet created by the cell is influenced by several factors that are intrinsic to the cell itself. Flagella magnitude l and average angle γ, mean swimming speed of the cell (V_s).

In conclusion, the viscosity of the live suspension is influenced by various factors such as the cells' swimming speed, flagella beating frequency, and amplitude. Temperature changes can also have an impact on these factors. Therefore, by measuring the cells' swimming speed and flagella beating frequency at different temperatures, we can gain insights into the relationship between temperature and the viscosity of the live suspension, as observed in previous research [24].

2.2.5. Swimming velocity responds to temperature

The term "Thermotaxis" signifies a movement of a living organism in response to heat stimulation [21]. Thermotaxis is not a unique trait of Chlamydomonas. It was first observed

in the unicellular slime mold [3]. Thermotaxis is a common mechanism employed by microorganisms and other small organisms to navigate toward more optimal temperatures. When *C. reinhardtii* is grown at different temperatures, it exhibits a tendency to move towards its preferred culturing temperature. For instance, if it is cultured at 20° and then placed into an environment with a higher or lower temperature, it will move towards the side that is closer to 20° [30]. The uniformity of ambient temperature during the experiment suggests that thermotaxis does not exert a dominant influence on the swimming behavior of the live algae suspensions.

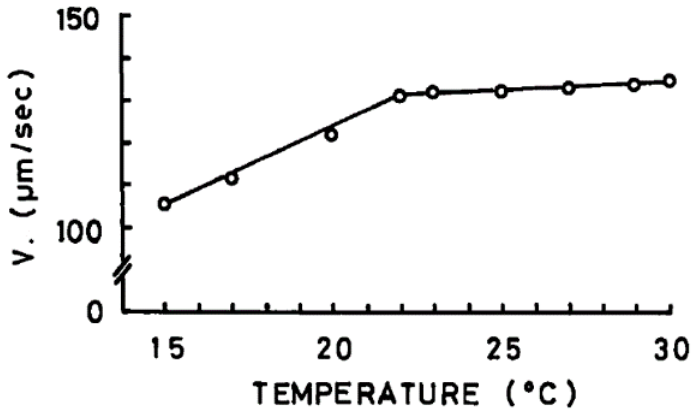

Figure 2.7: Swimming velocity of Chlamydomonas under different temperatures. Source: TOSHIKAZU [19].

As evidenced by previous literature, it was observed that the swimming velocity of cells exhibited an augmentation in response to elevated temperatures [19]. This phenomenon may potentially underlie the observed increase in viscosity.

2.3. Research goals

The present study aims to investigate the impact of temperature on the motility of *C. reinhardtii*. The first objective of this study is to characterize the effects of different temperatures on microalgal swimming speed. The second objective is to examine the flagella beating frequency in microalgal responses to temperature. Lastly, this study aims to investigate the influence of temperature on rheological properties, specifically focusing on viscosity modulation. To accomplish this research goal, several steps were carried out, including:

- To develop a temperature control system to regulate the temperature of the algae suspension.
- To perform 2D and 3D tracking of algae suspensions at different temperatures.

As this area of research has not been extensively studied, the findings from this study will provide essential insights into the motility of *C. reinhardtii* at different temperatures. These selected areas of investigation bear significant implications for enhancing microalgal cultivation, minimizing accumulation effects, and broadening the range of their potential applications.

3

Methodology & Experimental setup

The measurement of algae motility at various temperatures involves a closed-loop system that integrates several components, including temperature control mechanisms, water circulation systems, and a temperature chamber. Figure 3.1 is the schematic of the experimental setup. The subsequent sections will describe these systems in greater detail.

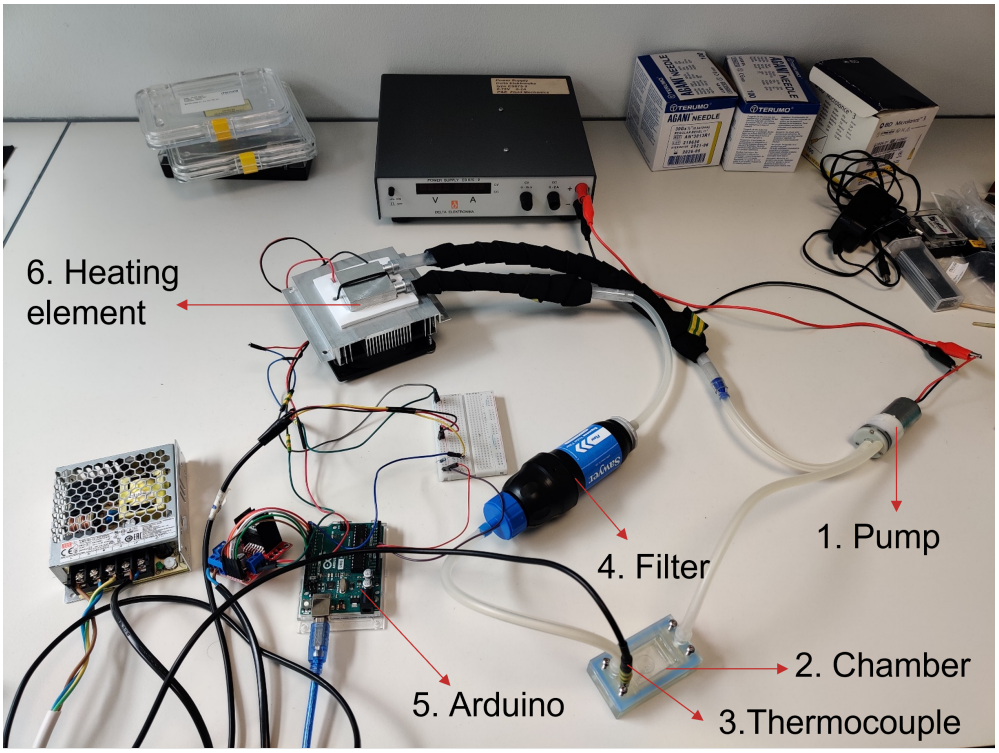

Figure 3.1: Experimental setup 1. Water pump 2. Temperature chamber 3. Temperature sensor 4. In-line water filter 5. Arduino Uno REV3 6. Peltier element.

3.1. Temperature control system

Temperature control is vital to our experiment because we will measure algae's motility in different temperatures. Temperature control is a group of bachelor's students initially designed for this experiment [13]. It uses a Peltier element to both cool and heat the circulation fluid.

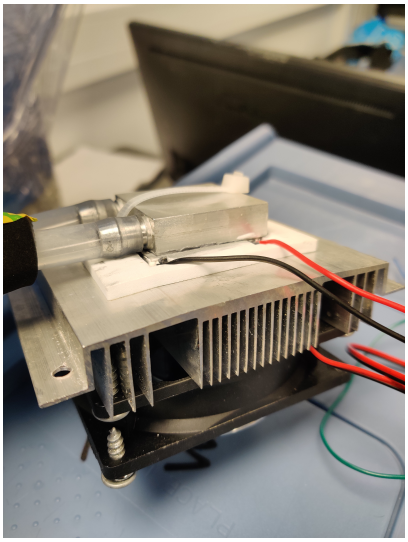

Figure 3.2: Peltier element integrated with heat sink. The power supply is connected to the red and black wires of the Peltier element, while the bottom part of the setup consists of a heat sink accompanied by a CPU cooling fan. This configuration serves to improve the heat transfer on one side of the element. On the other side of the element, there is contact with a metal heat exchanger, which facilitates the transfer of heat from the element to the circulating water.

A Peltier element (figure 3.2), known as a Peltier device or thermoelectric cooler (TEC), operates as a solid-state heat pump by utilizing the Peltier effect to establish a temperature gradient across its two sides upon the passage of an electric current. The Peltier effect, governed by the heat absorption or release at the junction of dissimilar materials upon the current flow, forms the basis of this phenomenon. Comprising two distinct semiconductor materials joined together at a junction. A Peltier element absorbs heat on one side and release heat on the other when an electric current is applied. It creates a temperature gradient that enables the Peltier element to function as both a cooler and a heater by reversing the direction of the current. This feature makes it suitable for cooling and heating applications in water circulation systems without additional component integration.

Peltier elements offer several advantages, including compact size, the absence of moving parts, and precise temperature control capabilities. However, it is crucial to note that effective heat dissipation is required on the hot side of the Peltier element to dissipate the generated heat. To enhance heat dissipation efficiency, a heat sink design was developed, providing an enlarged surface area for improved heat transfer. MX-4 thermal paste enhanced the thermal conductivity between the Peltier element and the heat sink. This paste fills microscopic imperfections at the interface, facilitating efficient heat transfer. MX-4 thermal paste, composed of non-conductive carbon-based materials, ensures that there are no risks of short circuits or damage to electronic components if it comes into contact with other sys-

tem parts. The Peltier element is connected to an L298N motor driver integrated circuit (IC) to control the Peltier element. The L298N is a widely used dual H-bridge motor driver IC that enables the control of direction and speed for DC motors. With its capability to handle high currents and operate within a broad range of input voltages, the L298N IC facilitates utilizing different voltage levels within the system.In this configuration, the Peltier element has a maximum working current of 3A, and the L298N motor driver can distribute the power under an Arduino's controllability.

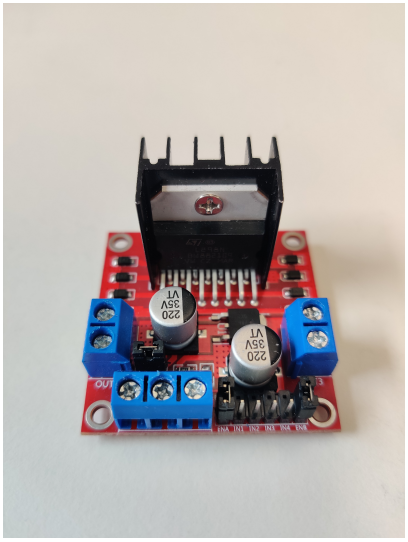

Figure 3.3: L298N dual H-bridge motor driver.

A thermocouple is connected to a Arduino to provide real-time temperature measurements. The Arduino then communicates with the L298N motor driver to regulate the power distribution to the Peltier element accordingly.

Verification of the heat balance of the system is essential to ensure a uniform temperature distribution in the flow cell. One approach to assess the uniformity of temperature distribution is by examining the Biot number. The Biot number is a dimensionless parameter that characterizes the relative contributions of conduction and convection in heat transfer processes.

$$Bi = \frac{\text{Thermal resistance for conduction inside the body}}{\text{Thermal resistance for convection at the surface of the body}} = \frac{hL}{k} \tag{3.1}$$

Where k represents the thermal conductivity of the material of the chamber body, with a value of 10^{-1} [W/(m·K)]. L denotes the characteristic length of the chamber, which is 10^{-3} [m]. h is a convective heat transfer coefficient [W/(m^2 · K)]. The thermal conductivity of water is approximately 10^{-1} [W/(m·K)], and the characteristic length of the chamber is 10^{-3} [m]. Given that the flow speed in the chamber is on the order of 10^{-1} [m/s], resulting in a Reynolds number of 10^3, the flow condition is still within the laminar flow regime, leading to a convective heat transfer coefficient h of approximately 10^1. Consequently, the order of magnitude of the Biot number in the system can be approximated as follows:

$$Bi = \frac{h}{k} \cdot L = 10^{-1} \tag{3.2}$$

When the Biot number is below approximately 0.1, it signifies that the internal conduction of heat within the body is much less significant compared to the convective heat transfer at the surface. This implies that temperature variations within the body can be considered negligible and therefore the temperature is uniform in the chamber. The experimental setup depicted in figure 3.5 involves the live suspension being enclosed within a 2mm thick acrylic plate, which is sealed using two coverslips. The flow cell exhibits symmetry in both the vertical and horizontal directions, allowing for a simplified one-dimensional heat transfer model, specifically from the top to the middle of the suspension (Elaboration on the finer aspects of the suspension will be provided in Section 3.5). Although temperature measurements are not conducted at every location, this assumption allows for simplifications in the analysis and interpretation of the experimental results. Once the target temperature is reached, we allow for a one-minute waiting period to ensure that the flow cell attains a uniform temperature similar to that of the chamber.

3.2. Temperature chamber design

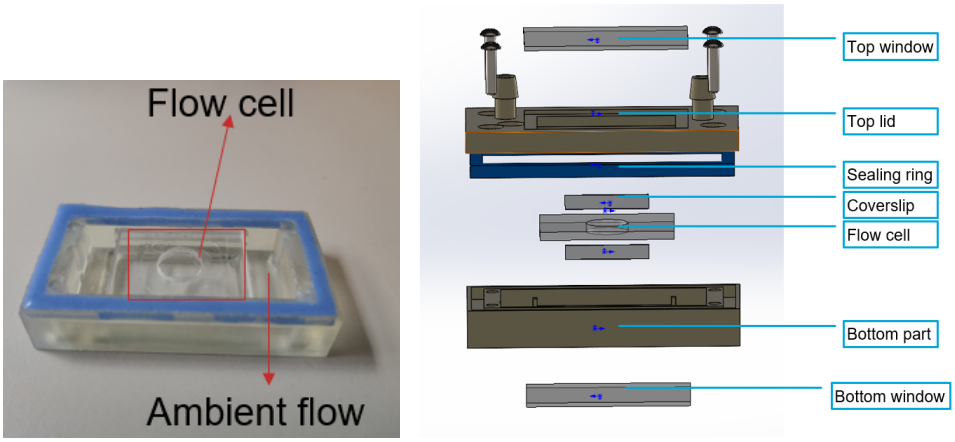

(a) Temperature chamber with flow cell

(b) Temperature chamber(disassembled)

Figure 3.4: Temperature chamber design.

The flow chamber plays a critical role in this experiment, serving as the container for the algae cells under investigation. It comprises two parts, a top lid and a bottom sink which can be easily assembled, top lid has a water inlet and outlet to ensure the water can circulate continuously inside the chamber. The flow cell has to be placed in the bottom part before assembling them. Additionally, the chamber is optically accessible from the bottom, facilitating easy camera observation, while laser illumination can penetrate the entire chamber from the top. To ensure the chamber is watertight, we use UV glue to bond two glass slides to the chamber and adhered to both the top lid and bottom sink. Furthermore, a food-grade sealing ring was used prevent leaks from the side of the chamber. These details are highlighted in Figure 3.4. The coverslips themselves have a thickness ranging from 0.13mm to 0.17mm, while the suspension has a uniform thickness of 1mm. In our experimental procedure, we assume that the temperature distribution within the temperature chamber is homogeneous

throughout. This assumption is based on the consideration that the Biot number, which characterizes the relative rates of heat transfer within a system, is approximately 0.1.

The temperature in the temperature chamber is controlled using a temperature sensor known as ”DS18B20”. This sensor has a temperature range of -50 to 120 degrees Celsius and can measure temperature with a resolution of 0.5 degrees. The sensor is inserted from the top lid of the chamber and provides real-time feedback to the Arduino, enabling precise temperature control in the chamber.

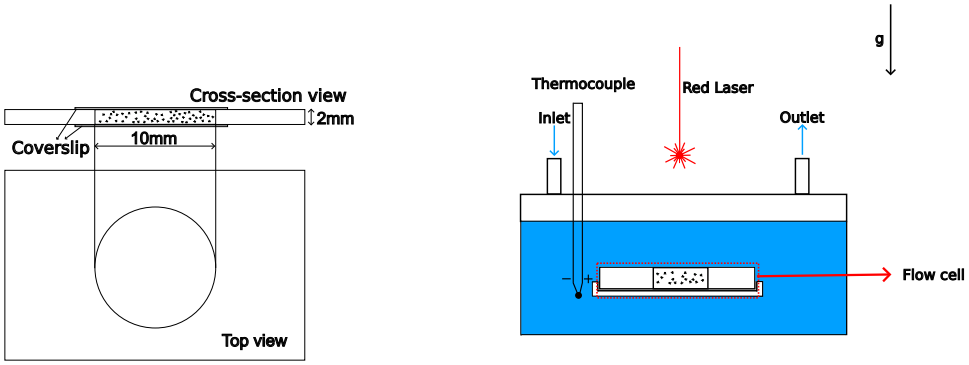

(a) Flow cell (b) Temperature chamber

Figure 3.5: Cross-sectional view of temperature chamber and flow cell dimensions.

The positioning of the flow cell is depicted in the figure 3.5, which is crucial in this study as it serves to isolate the algae cells from the surrounding ambient flow. This isolation enables precise control of the temperature of the cells' swimming environment without external interference. A schematic representation of the flow cell is presented in figure 3.5, providing insight into the dimensions and overall appearance of the flow cell.

3.3. Water circulation system

The ambient water flow is important in transporting heat from the Peltier element(tec1-12704, 12V 36W) to the temperature chamber and maintaining temperature stability. Therefore, it is essential to have a water pump that can provide an adequate flow rate in the system. The ”Dilwe RC Boat Water Pump” was selected for this experiment, as it can provide a flow rate ranging from 200ml to 600ml per minute, ensuring an efficient flow rate in the water loop circulation. Figure 3.1 shows the various components integrated into the water circulation system, and after integrating all the parts, the flow rate remained stable within the range of 200ml to 400ml per minute.

After the initial experiments, an in-line filter was installed in the system to address the issue of particle contamination in the ambient flow. The filter was deemed necessary as the flow often contained numerous particles that could adversely affect the tracking code analysis. Despite the fact that these particles were not visible to the naked eye, their presence could significantly impact measurements, given the small size of the *C. reinhardtii* cells (10

Figure 3.6: In-line water filter. Pore size 0.1 microns, Source: Sawyer [34].

microns). The filter was selected for its uniform pore size of 0.1 microns, which has been shown to remove 99.9999% of bacteria and protozoa, including E. coli, giardia, and cryptosporidia [34].

To minimize heat loss from the water tubes, a layer of heat insulation foam is applied to cover the tubes. This insulation reduces the transfer of heat from the water inside the tubes to the surrounding environment. The insulation foam helps maintain the desired water temperature within the system by creating a barrier that limits heat conduction and convection.

3.4. Tracking system

In our study we use two different tracking systems: the 2D and 3D microscope tracking system. Each tracking system includes the hardware tracking aspect, and the tracking code, which encompasses the software tracking.

The LaVision imager sCMOS camera incorporates a state-of-the-art scientific CMOS (sCMOS) sensor that combines the strengths of modern CCD and CMOS technologies. The individual pixels in the camera sensor measure 6.5×6.5 μm in size, enabling precise capture and representation of the observed suspension. With its frame rates of 50 Hz at full resolution, the Imager sCMOS camera is particularly well-suited for flow field imaging applications, providing excellent Particle Image Velocimetry (PIV) performance [16]. To improve the imaging capabilities of both the 2D and 3D microscopes, we integrate the Imager sCMOS camera. This integration enhances our ability to obtain precise and comprehensive visual information for our research and analysis.

3.4.1. 2D Microscope

2D microscope refers to the ECLIPSE Ti2 inverted microscope, its distinctive hardware-triggering capabilities further enhance the performance of even the most demanding high-speed imaging applications [23].

To accurately track the micron-scale algae cell body and its flagella, we have selected a 20x lens to ensure sufficient magnification for obtaining sharp images. The layout of the experimental setup depicting the positioning of the lens and other relevant components can be observed in the accompanying figure 3.8.

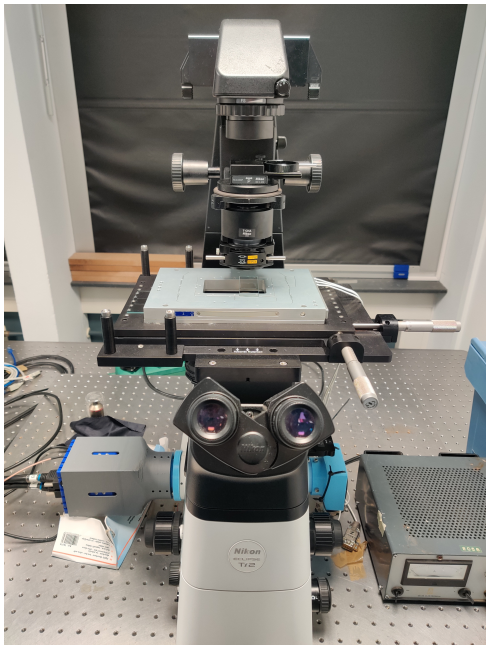

Figure 3.7: Nikon ECLIPSE Ti2 inverted microscope.

Based on previous research that has established the flagella beating frequency of live *C. reinhardtii* to be around 50-60 Hz [14], it is crucial to adhere to the Nyquist condition to avoid aliasing during signal measurement. The Nyquist condition states that the sampling frequency should be at least twice the signal frequency ($f_{\text{sampling}} \geq 2f_{\text{signal}}$). In order to ensure accurate measurements, it is advantageous to have a higher sampling frequency. However, it is important to note that increasing the recording rate of the camera results in a smaller field of view (FOV), as fewer pixels are active at any given time. To strike a balance between the recording rate and FOV, we have chosen a resolution of 480×480 pixels and a recording rate of 450 frames per second (FPS) for our setup. This selection allows for a compromise between capturing a sufficiently high sampling frequency and maintaining a reasonable FOV for effective tracking and analysis of the flagella movement.

3.4.2. 2D Tracking algorithm

The 2D tracking algorithm is derived from the 3D tracking algorithm with specific modifications. It utilizes minima and maxima criteria to detect algae cells. However, specific initial settings need to be specified for the 2D tracking algorithm due to changes in magnification, recording rate, and resolution from the 3D tracking setup. These initial settings include parameters such as the number of pixels required to detect a single algae cell, pixel size (which affects the spatial resolution), frames per second (fps) for recording, and other relevant parameters. These settings are crucial for accurately detecting and tracking algae cells in the 2D tracking system, as they determine the resolution, temporal sampling, and sensitivity of the algorithm to capture the desired cell movements and behaviors.

In Figure 3.9, the visibility of the flagella of the algae cell is limited. This is primarily attributed to the shallow depth of field when using an inverted microscope with a 20x lens, which typically ranges from 20 to 50 micrometers. Since the live algae cells can freely swim

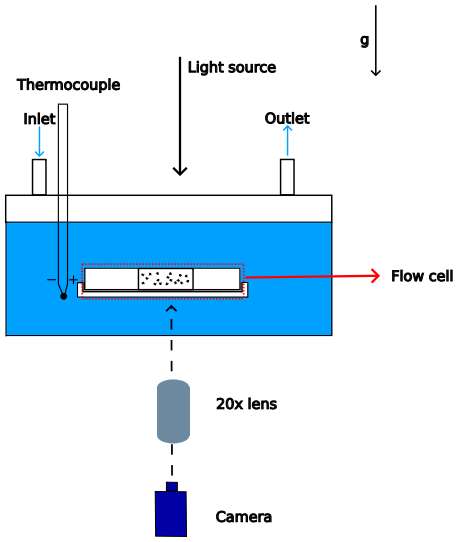

Figure 3.8: Cross-sectional view of temperature chamber and flow cell on 2D microscope. The light source used in 2D tracking is provided by an inverted microscope equipped with a 20x lens. By using a single camera, we are able to measure the beating frequency of the algae cells. This setup allows for accurate and precise observation and analysis of the cell's motion and provides valuable data on their motility characteristics.

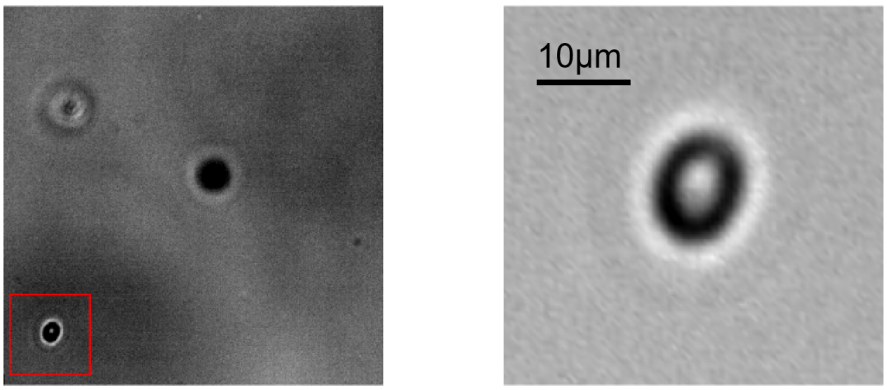

Figure 3.9: Tracking and detection of live cell in 2d tracking algorithm.

within the flow cell, they often move out of the focal plane, making it challenging to track the flagella over extended periods of time. However, we can still calculate the flagella's beating frequency by observing the algae cell's body movement. Despite being out of focus, the body movement of the cell exhibits a continuous back-and-forth motion, as depicted in Figure 3.10. The net displacement of the cell is in a forward direction, and each complete back-and-forth movement corresponds to an entire beating cycle of the flagella. Therefore, by analyzing the body movement of the cell, we can indirectly estimate the beating frequency of the flagella. This approach is feasible because the swimming environment is characterized as inertia-free, as discussed in Section 2.1.3.

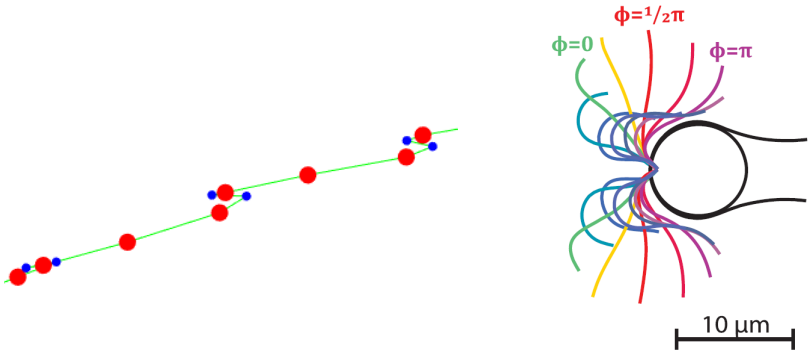

(a) Cell body back-and-forth movement

(b) Flagella movement. Source: Wei[39]

Figure 3.10: Swimming motion and flagella beating cycle.

3.4.3. 3D Microscope

Figure 3.11 represent the 3D microscope, it utilized in our study employs four cameras positioned at distinct angles to capture the target object from multiple perspectives. This configuration enables the generation of a comprehensive three-dimensional profile of the suspension, this will encompass details concerning the object's three-dimensional position and velocity information. The light source utilized in 3D tracking is a red laser as shown in figure 3.12, chosen for its increased power and ability to directly illuminate the flow cell. Employing a red laser serves the purpose of circumventing potential phototaxis in algae cells, as phototaxis has the potential to influence the measurement results of motility [36]. This setup enables the capture and analysis of the swimming velocity of the cells within a three-dimensional domain.

During the experiment, all internal lights in the laboratory are turned off to minimize ambient glare. Instead, the red laser is switched on to provide illumination. This helps to reduce any potential interference from external light sources. Additionally, the position of the temperature chamber can be adjusted slightly using the 2-axis wheel, as depicted in the figure 3.11.

The selection of a low frame rate (20FPS) in the 3D microscope aims to reduce the data size during extended recording periods lasting from 3 to 5 minutes. This choice facilitates the capturing of prolonged trajectories of individual cells, thereby enabling a more comprehensive analysis of behavioral patterns and the evaluation of motility in algae cells. To capture the desired field of view, the area of interest for all four cameras has been configured to 640×640 pixels. The depth of field in the 3D microscope is set at 2mm, ensuring that all cells within the flow cell are adequately covered. It is important to note that the 3D microscope has a lower magnification (1.5x) compared to a 2D inverted microscope. When employing dark field imaging, cells observed under the 3D microscope appear as white dots. However, it is worth mentioning that flagella movements cannot be visualized using the 3D microscope. Consequently, the primary capability of the 3D microscope is restricted to tracking the movement of the cell body rather than flagella movements.

Figure 3.11 illustrates the integration of a red laser with the 3D microscope. The laser

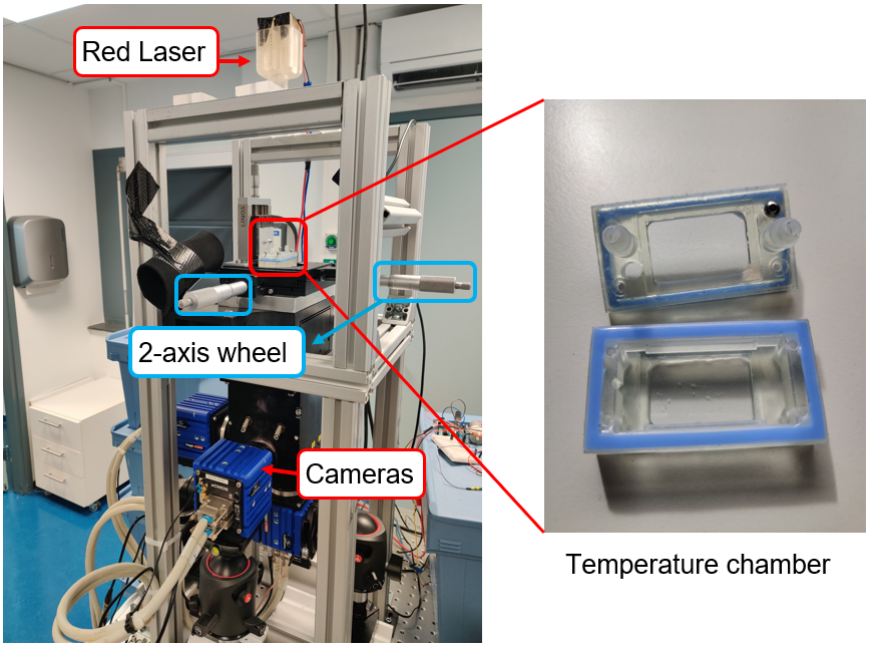

Figure 3.11: 3D microscope. A red laser is positioned at the top of the entire configuration. Four cameras are situated at the bottom, each set at a distinct angle. The red square in the diagram highlights the location of the temperature chamber within the setup.

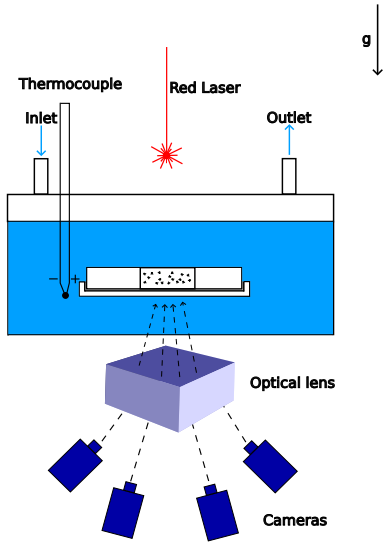

Figure 3.12: Cross-sectional view of temperature chamber and flow cell on 3D microscope.

emits light with a wavelength of 650nm, specifically chosen to minimize the phototactic movement of live algae cells.

3.4.4. 3D Tracking algorithm

The initial data acquisition is performed using DaVis10, a commercial software that is used for recording of the four-camera system at specific recording rates and resolutions. Once the raw data is obtained from DaVis10, it is converted into the im7 format and imported into MATLAB for further analysis. We used a customized tracking algorithm developed by Koen Muller [20]. It offers the flexibility to customize specific settings according to the requirements of individual experiments. This adaptability allows researchers to tailor the algorithm parameters to suit their specific experimental conditions, ensuring optimal tracking performance and accurate analysis of the data. For instance, various recording parameters such as recording rate, resolution, pixel size, object size, light intensity, and field of view are incorporated within the settings, allowing for customization tailored to specific recording data requirements.

The 3D tracking algorithm is based on capturing light-intensity contrasts between cells and backgrounds. As previously mentioned, cells appear as white dots in the images due to the adoption of the ”maxima” criteria for tracking. This criterion tracks pixels that have reached their maximum value. In this case, four pixels can represent a single cell. By specifying an acceptable range for the number of pixels and applying appropriate filters, irrelevant particles that do not meet the correct size criteria can be effectively filtered out during the analysis process.

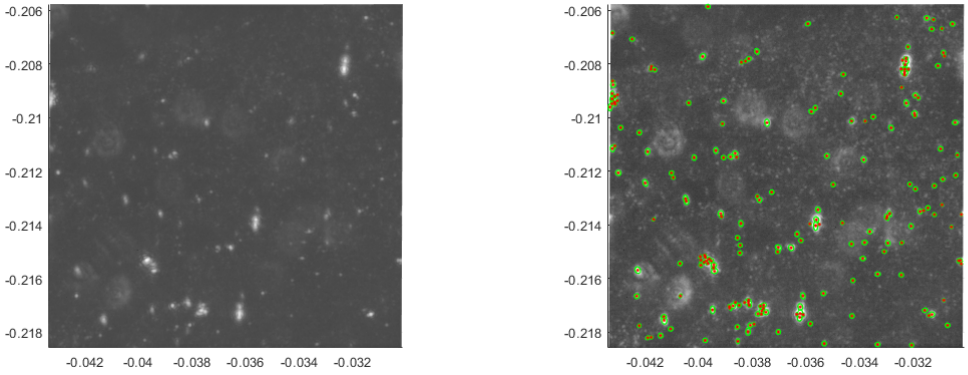

(a) Raw image (b) Tracked algae cells

Figure 3.13: Detection of live cells from raw image.

Figure 3.13 displays the presence of halo-like bright dots, which are air bubbles present in the ambient water flow. These air bubbles tend to adhere to the exterior surface of the coverslip. To minimize the occurrence of air bubbles in the ambient flow, we degas the water before experimenting. This degassing process helps to reduce the amount of dissolved air in the water, thereby minimizing the formation of bubbles.

Additionally, small white dots are not detected in the image. These dots correspond to dust particles that have settled on the coverslip. However, these dust particles have sizes distinct from the live cells, enabling the filtration of most of these irrelevant particles. Applying appropriate filtering settings in the code allows these dust particles to be effectively

excluded from the analysis, focusing solely on the relevant cell data.

3.5. Algae culture

Algae cells are conventionally preserved within a solid medium for prolonged usage, owing to the relatively slower growth rate of algae cells within solid media than in liquid media. This attributes solid medium as a source for continuously cultivating algae cells. When preparing for experiments, the algae cells are cultured in a liquid medium known as ”Tris”. Tris(hydroxymethyl)aminomethane is a commonly employed buffer in the field of biological and biochemical research. Its primary function is to maintain a stable pH environment, making it a valuable component in cell culture and molecular biology experiments. Tris can also serve as a component of growth media for specific cell types, providing an optimal environment for cell growth while ensuring pH stability. Tris-based media are frequently employed in the cultivation of various mammalian cells, including cell lines and primary cells.

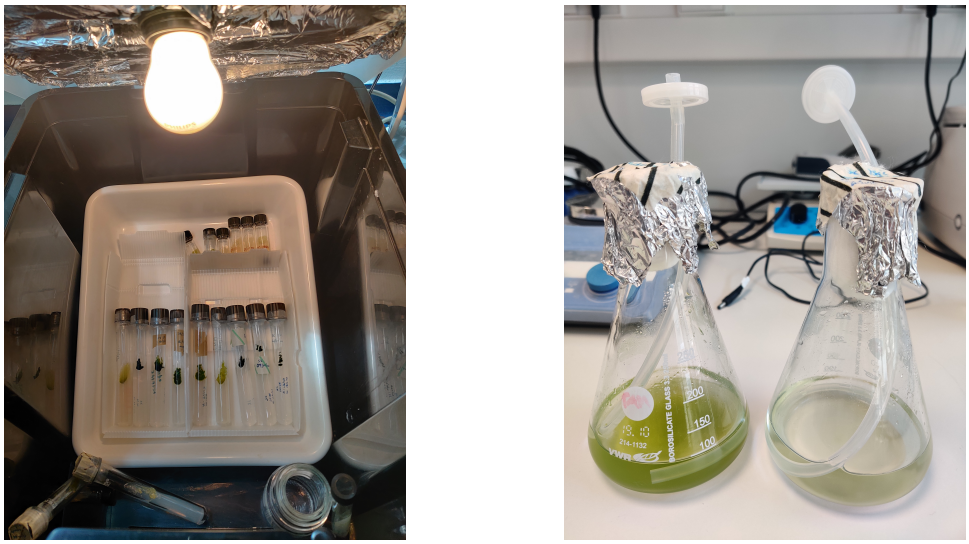

(a) Solid culture medium

(b) Liquid culture medium

Figure 3.14: Algae cell culture medium.

In the growth box, a light cycle of 14 hours on and 10 hours off is maintained daily to simulate natural light conditions. The air is continuously pumped into the Erlenmeyer flask to ensure an adequate supply of carbon dioxide (CO2) for the algae cells. After four days of cultivation, the cell density reached approximately 10^5 live cells per ml, determined using a Neubauer counting chamber 3.15.

A culture check is conducted under an inverted microscope to verify the cells' viability and health. Several criteria are examined, including maintaining a room temperature of 20-25 degrees Celsius, flagella beating frequency ranging between 50-60 Hz, and a swimming velocity of approximately 100 microns per second. Once multiple live cells are confirmed, the suspension is diluted to a concentration of 10^4 cells per ml. Since the flow cell can accommodate only 0.15 ml of live suspension, it will contain a total of 10^3 cells, including a

(a) Neubauer counting chamber (b) Micropipette

Figure 3.15: Methods for quantifying cell density and manipulating small volumes of cell suspensions. These instruments enable researchers to accurately determine the concentration of cells in a given sample and perform precise transfers of minute volumes of cell suspensions.

few hundred live cells. To extract 0.15 ml of live suspension, a micropipette 3.15 is employed with a slow flow rate to minimize the shear stress from the pipette wall, thereby reducing the number of deflagellated cells.

4

Results

This chapter presents the results of the temperature control experiments. We report the beating frequency of algae cells' flagella, and swimming velocity measurement. The calculation of stresslet strength will be discussed in section 5.

4.1. Outcome of Temperature Regulation

We begin by finding the optimal settings for temperature control within the chamber. The Ziegler-Nichols method is a well-known approach for determining a temperature control system's proportional-integral-derivative (PID) gains. This technique involves performing step tests on the system and utilizing the response data to calculate the appropriate gains for the PID controller. The proportional (P) term provides an output proportional to the current error (the difference between the setpoint and the process variable). A higher proportional gain (Kp) results in a more robust response to the present error, which helps reduce the error but may lead to overshoot and oscillations. The integral (I) term considers the accumulated error over time and aims to eliminate steady-state errors. It helps to correct any long-term bias in the control variable by gradually adjusting it based on the accumulated error. The integral gain (Ki) is used to control the strength of this corrective action. The derivative (D) term considers the rate of change of the error and provides a corrective action to anticipate and counteract potential future changes. It helps to dampen the response, reducing overshoot and oscillations. The derivative gain (Kd) is used to control the strength of this anticipatory action. The following steps can be implemented to use the Ziegler-Nichols method:

Firstly, set the integral and derivative gains (Ki and Kd) to zero, and assign a small value (e.g., 1) to the proportional gain (Kp). Secondly, increase the setpoint by a small amount (e.g., 5°C) and wait for the temperature to stabilize at the new setpoint. Thirdly, suddenly change the proportional gain (Kp) to a higher value (e.g., double the previous value). Fourthly, monitor the temperature response and record the rise time (Tr), which is the time required for the temperature to reach the new target temperature, and the peak time (Tp), which is the amplitude of the first overshoot. After determining the rise and peak times, the following

formulas can be employed to calculate the PID gains: Kp = 0.6Kc, Ki = 1.2Kc/Tr, and Kd = 0.075Kc×Tp. Here, Kc represents the critical gain that generates sustained oscillations in the system, and it can be estimated as Kp when the system starts oscillating. In this scenario, coefficient Kc's value is established by determining Kp, set at 255, representing the uppermost admissible input to ensure the attainment of the maximum heat flux. The gains can be adjusted by fine-tuning them up or down and observing the temperature response, using trial and error or other tuning techniques. It is crucial that the Ziegler-Nichols method provides a valuable starting point for tuning the PID gains. However, it may only be suitable for specific temperature control systems. Because different ambient temperatures can have different heat loss. Therefore, evaluating the control performance under various scenarios is recommended before deploying the system in other real-world applications.

Figure 4.1 indicate the temperature control between the initial setting and the setting with the optimal Ki and Kd values. The Arduino code will be provided in the appendix A for reference.

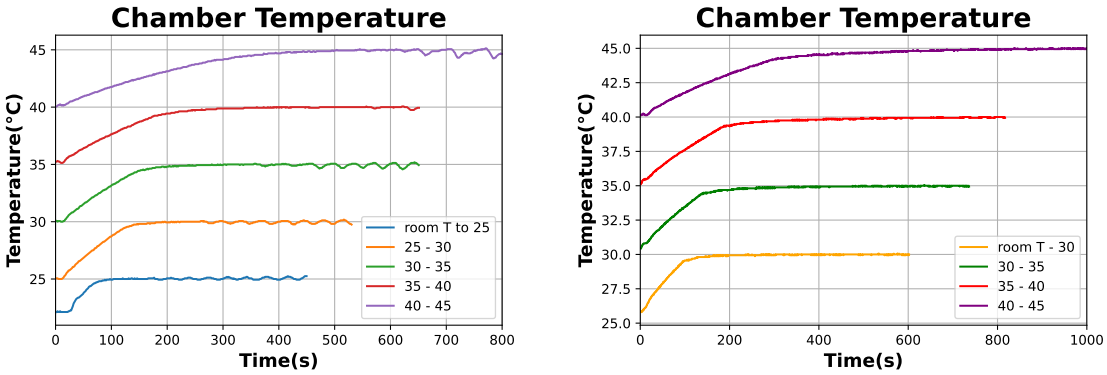

(a) Initial temperature control

(b) Damped temperature control

Figure 4.1: Temperature in the flow chamber.

For achieving optimal control in both the cooling and heating processes, the proportional-integral-derivative (PID) gains have been determined as follows: kp = 255, ki = 1, and kd = 20. It is important to note that these specific values are only suitable for the particular experimental conditions, encompassing the setup's room temperature, Peltier element type, flow rate, and overall heat resistance. These gains have been optimized for this specific regime to ensure effective temperature regulation and should be adjusted accordingly if any of the mentioned parameters undergo substantial changes.

4.2. Quantification of Flagella Beating Frequency

Figure 4.2 illustrates the 2D tracking results for a live algae cell, including swimming speed calculations, trajectories within the full image, and instant speed to describe the back-and-forth movement and the resulting beating frequency. The swimming speed of the algae cell is determined by measuring the overall path covered by the cell within a single plane, taking into account the camera's recording time. It should be noted that since the algae cell may occasionally move out of focus, the calculated swimming speed serves as a reference

and is not included in the analysis of swimming velocity.

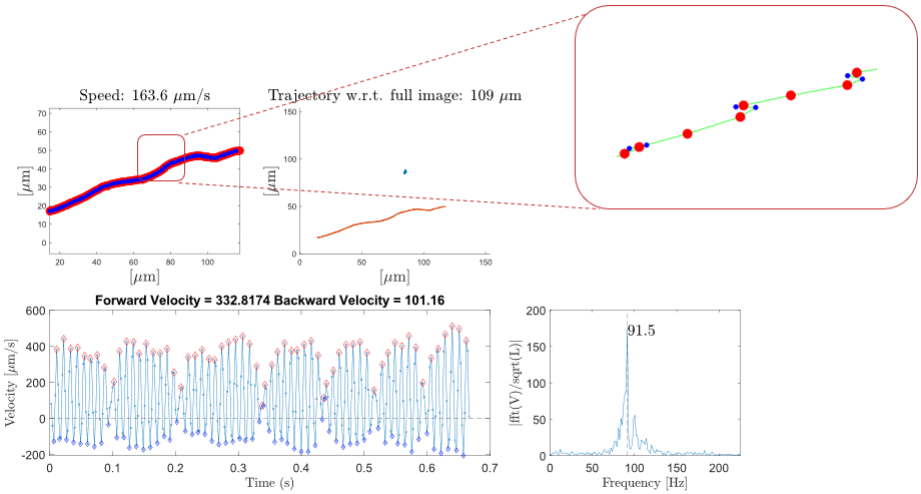

Figure 4.2: 2D tracking result for a single cell at 30 degrees Celsius.

During the experiment, recordings were conducted at each temperature ranging from 15 to 40 degrees Celsius, in increments of a 5-degree. Due to limitations in the temperature control system, the minimum temperature achievable within the temperature chamber is 13 degrees Celsius. Therefore, it was decided to initiate the measurements from a temperature of 15 degrees Celsius to ensure accurate and reliable data collection within the feasible temperature range of the experimental setup. At the highest temperature of 40 degrees Celsius, the algae cells displayed abnormal behavior characterized by erratic movements of their flagella. This led to difficulties in synchronization, and their swimming speed became unstable. After 10 minutes of exposure to 40 degrees Celsius, a significant portion of the cells, approximately 99% had succumbed to these adverse conditions and died. Consequently, no further experiments were conducted at temperatures above 40 degrees Celsius due to the high mortality rate observed among the algae cells. At least ten different cells from various culture days were observed and recorded for every temperature point.

From Figure 4.3, it is evident that temperature plays a critical role in influencing the frequency of flagella beating in the cells. The observed flagella beating frequencies range from approximately 30 Hz to a maximum of around 90 Hz. Notably, a distinct peak in flagella beating frequency is observed at a temperature of 35 degrees Celsius. This finding suggests that 35 degrees Celsius is a temperature point at which the flagella beating frequency reaches its highest value within the investigated temperature range.

When comparing the beating frequency results with Figure 2.4, it becomes evident that they exhibit a similar trend of increase from 15 to 35 degrees Celsius, with a peak value observed at 35 degrees. This initial experimental finding provides evidence to support the hypothesis that live cell motility is related to the viscosity of the live suspension. To further investigate this relationship and provide a more detailed analysis, a quantitative analysis will be presented in Section 5. This analysis offers quantitative insights and a deeper understanding of the correlation between flagella beating frequency and the viscosity of the live suspension.

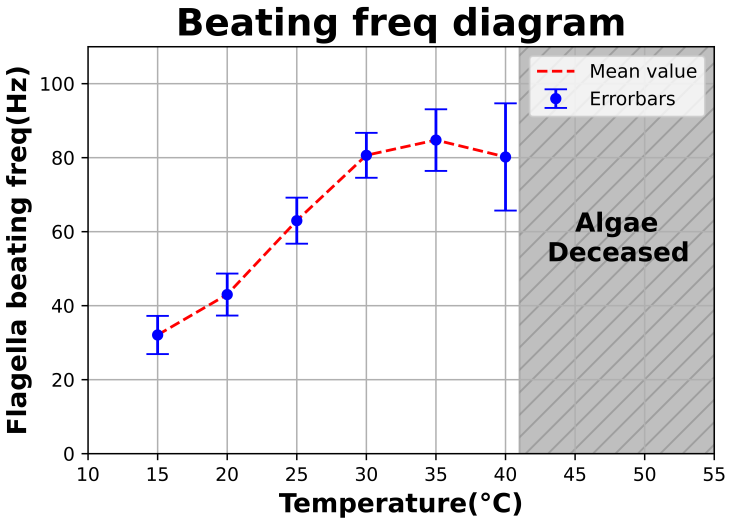

Figure 4.3: Live algae cells beating frequency at different temperatures.

4.3. Outcome of Swimming Velocity Analysis

In order to determine the swimming velocity, it is crucial to identify the trajectories that accurately represent the movement of live algae cells while excluding trajectories of dead cells or irrelevant particles. A control group was established to account for the potential influence of background flow and passive particles within the flow cell. In this control group, the focus was solely on measuring the movements of passive particles present inside the flow cell. All other experimental parameters were kept constant, except for substituting live algae cells with passive particles with similar size and density characteristics. This control group allows for comparative analysis, enabling the differentiation between the effects attributed to the background flow and the specific behavior of the live algae cells.

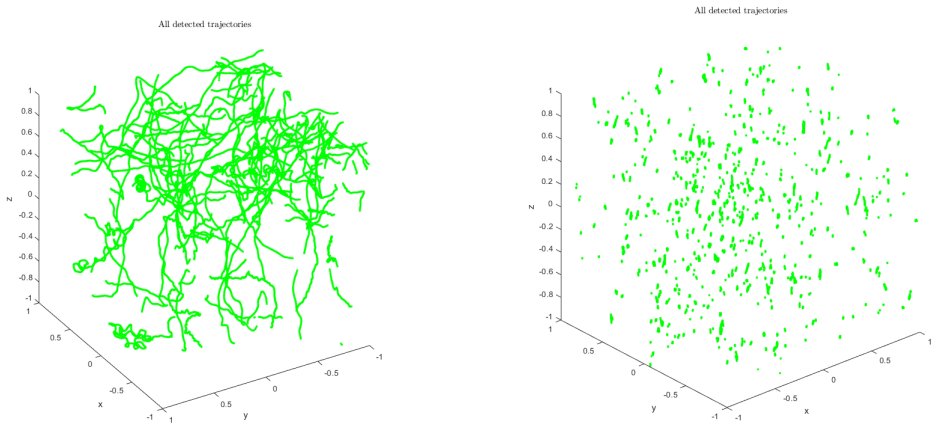

(a) Trajectories of live cells

(b) Trajectories of passive particles

Figure 4.4: Trajectories of live cells and passive particles at 35 degrees Celsius.

Figure 4.4 presents two sets of experimental results at the same temperature. The left-

hand side displays the swimming trajectories of live cells, while the right-hand side only shows passive particle trajectories of movement due to the background flow. A clear distinction can be observed between the trajectories of live cells and passive particles. Based on this distinction, specific criteria can be established to filter out the irrelevant trajectories based on the characteristic patterns exhibited by the trajectories of passive particles. Implementing such criteria makes it possible to selectively analyze and calculate the swimming velocity of the live algae cells while excluding trajectories that do not correspond to their movements. This approach ensures that the swimming velocity calculations are accurately derived from the relevant and representative trajectories of the live cells.

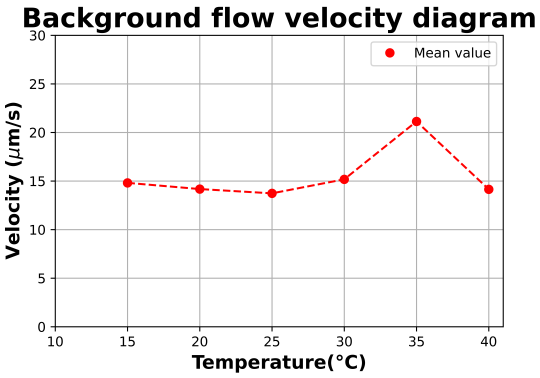

Figure 4.5: Pure passive particle velocity at different temperatures.

After applying the filtering procedure to remove irrelevant trajectories, a comparison of the same group of data allows us to observe the live cell swimming velocity at 35 degrees Celsius. By focusing on the relevant trajectories, which are created by live cells, and excluding irrelevant ones, which are created by passive particles and dead cells, we can obtain a more accurate assessment of the swimming velocity exhibited by the live algae cells at this specific temperature. Analyzing the filtered data enables us to discern the precise swimming velocity and explore any trends or patterns associated with the swimming behavior of the cells at 35 degrees Celsius.

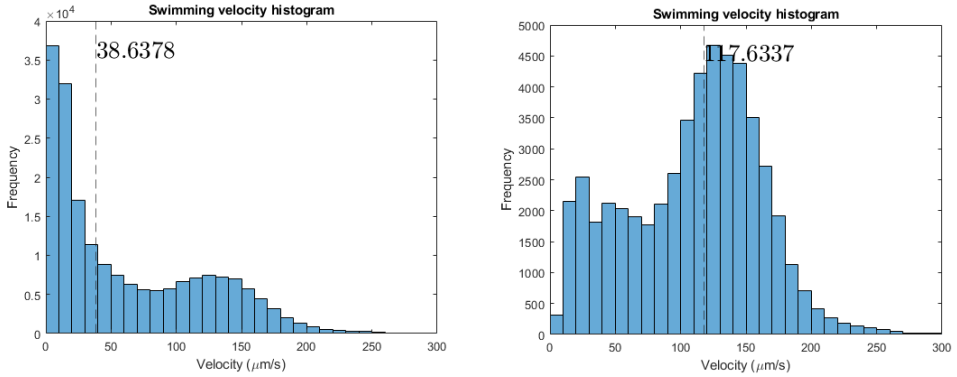

(a) Unfiltered swimming velocity

(b) Filtered swimming velocity

Figure 4.6: Swimming velocity between unfiltered and filtered data at 35 degrees Celsius. The dashed line represents the median value of the whole data set.

In Figure 4.4, numerous trajectories of live cell tracking are observed. However, when examining the swimming velocity distribution, the occurrence frequency appears to be in the order of thousands to tens of thousands. It is important to note that the swimming velocity plot does not represent a histogram of different trajectories. Rather, it represents a histogram of each individual data point in the velocity matrix. The velocity matrix collates computed velocities from sequential frame pairs within individual trajectories. This approach facilitates the tracking of velocities for each distinct trajectory. However, the overall swimming velocity plot is generated by aggregating velocities from all trajectories. This approach was chosen to overcome the limitation of having only a few tracks in certain outcome data, and a more comprehensive analysis can be achieved by plotting each data point's velocity for every track. Interpreting trends based on a limited number of data points can be challenging, but by considering each velocity point individually, a clearer understanding of the overall swimming velocity distribution can be obtained.

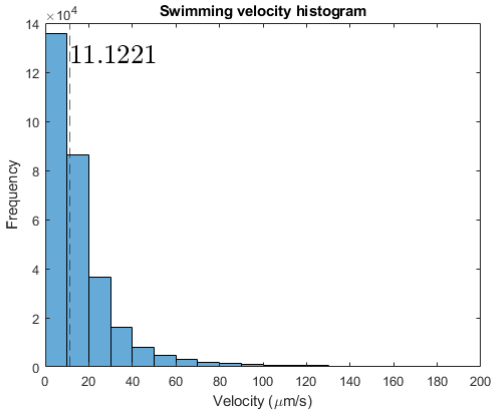

Figure 4.7: Pure passive particles velocity distribution at 35 degrees Celsius.

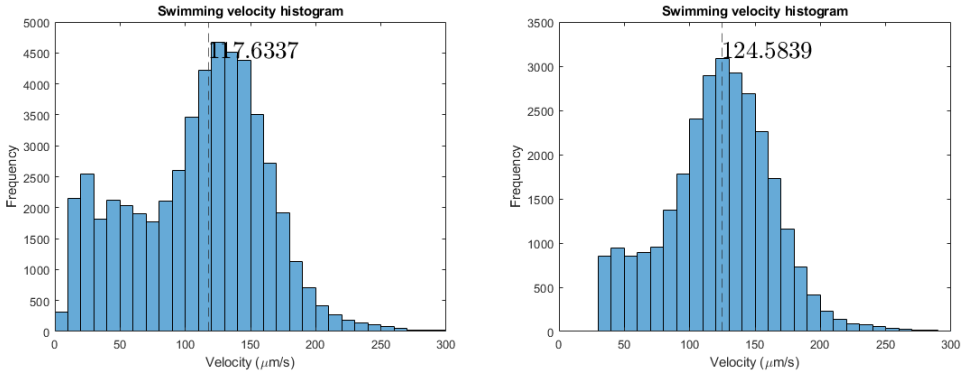

(a) Filtered swimming velocity (b) Final swimming velocity

Figure 4.8: Swimming velocity between filtered data and final result at 35 degrees Celsius.

Despite the best efforts to apply an efficient filter, it is important to acknowledge that the filtering procedure may not always be 100% effective, and a few (less than 10% of all trajectories) irrelevant trajectories may still be included in the calculated swimming velocity. To mitigate the potential influence of these remaining irrelevant particles, an additional step

was taken to measure the swimming velocity of pure passive particles as shown in figure 4.7. By measuring the swimming velocity of pure passive particles separately, it becomes possible to establish a baseline or reference value for the swimming velocity solely attributed to these particles. This allows for more accurate differentiation between the contributions of live algae cells and irrelevant particles to the overall swimming velocity observed in the experimental data.

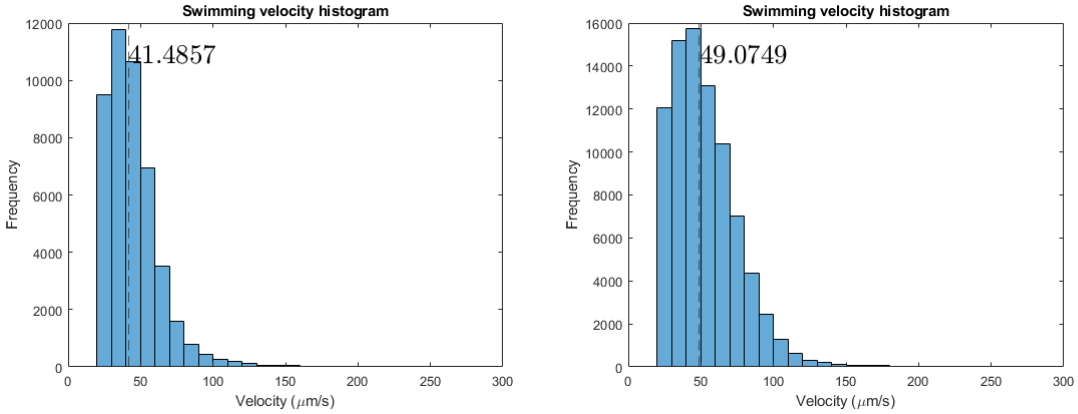

(a) 15 degrees Celsius

(b) 20 degrees Celsius

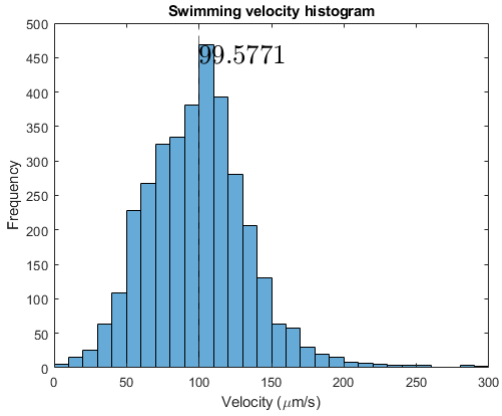

(c) 25 degrees Celsius

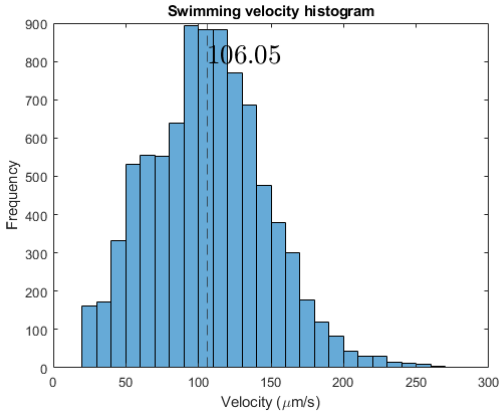

(d) 30 degrees Celsius

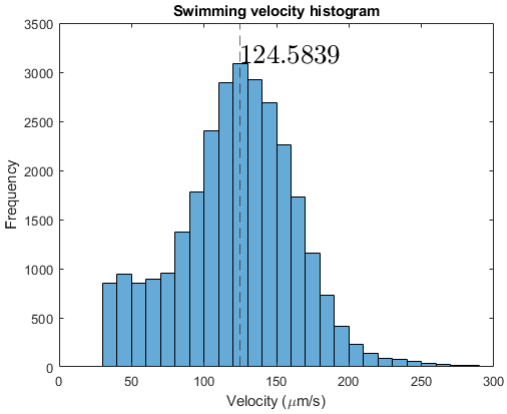

(e) 35 degrees Celsius

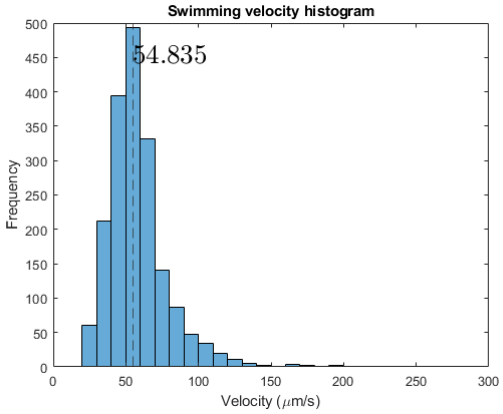

(f) 40 degrees Celsius

Figure 4.9: Swimming velocity distribution at different temperatures. The dashed line represents the median value.

Upon measuring the swimming velocity of pure particles at 35 degrees Celsius from figure 4.7, it was observed that the majority of these particles (10^4 times) exhibited velocities below 30 microns per second. As a result, to obtain a more accurate estimation of the actual swimming velocity of the live cells, we decided to disregard any swimming velocities below 30 microns per second at 35 degrees. By neglecting the swimming velocities below this threshold, we aim to minimize the potential influence of the slower-moving particles, which are dead algae cells and passive particles, on the swimming velocity analysis.

In Figure 4.9, each sub-figure corresponds to a final swimming velocity distribution at a specific temperature. The dashed line in each plot represents the median value of the data shown in that particular sub-figure. It is important to note that each plot represents a single group of data, specifically one temperature and one experiment. In some sub-figures, the velocity of passive particles at the corresponding temperatures is subtracted from the measured velocities of live cells. The velocity values of passive particles at each temperature are included in the appendix for reference and comparison purposes.

To obtain Figure 4.10, the data obtained for multiple experiments at each temperature are combined. Figure 4.10 provides a comprehensive overview by presenting the combined data from various experiments for each temperature. This allows for a more thorough analysis and comparison of the swimming velocity distributions across different temperatures.

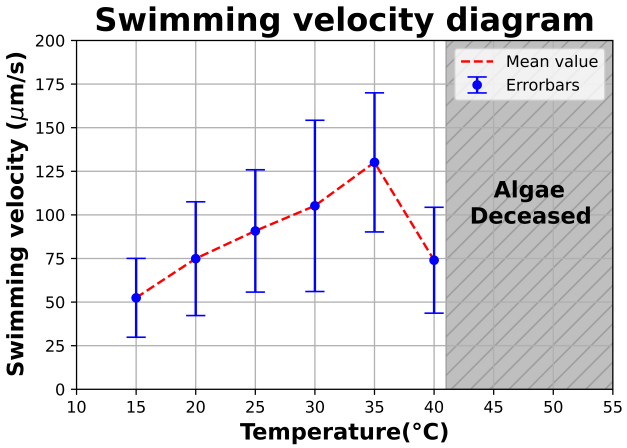

Figure 4.10: Swimming velocity distribution from 15 to 40 degrees Celsius.

Hundreds of cells from different days of culture were recorded at each temperature. The analysis of Figure 4.10 reveals that the swimming velocity of live cells increases from 15 to 35 degrees Celsius, reaching its peak at 35 degrees. However, at 40 degrees, the swimming velocity decreases. The lowest mean velocity is observed at 15 degrees, while at 35 degrees, the mean velocity is nearly twice the value of the lowest mean velocity. The standard deviation of the mean velocity is highest at 30 degrees, but it does not significantly affect the overall trend of the swimming velocity.

When comparing these findings with Figure 2.4, it becomes apparent that the two sets of data exhibit a similar increasing trend from 15 to 35 degrees Celsius. This correlation provides additional evidence to support the hypothesis that the motility of live cells impacts the rheological properties of the medium, particularly viscosity.

5

Discussion

5.1. Motility at different temperatures

We have analyzed the motility of algae cells by considering two main aspects: swimming velocity and flagella beating frequency. Due to the limited depth of field of the inverted microscope, the number of live cells swimming within the interrogation window is relatively small, even if the live cell suspension is not diluted. Typically, only one or two live cells can be observed swimming simultaneously in the interrogation window. As previously mentioned, the beating frequency results at each temperature are derived from at least ten different live algae cells, ensuring reasonable and reliable outcomes are generated. However, other statistical methods, such as calculating mean values and standard deviations, can still be utilized to gain valuable insights into the trend and variability of the flagella beating frequency at different temperatures.

The limited availability of motility measurement results of *C. reinhardtii* at different temperatures underscores the significance of this research. The findings presented in this study can serve as valuable resources for researchers working in relevant fields, facilitating a better understanding of *C. reinhardtii* behavior. The insights gained from this research can guide researchers in designing experiments and developing further investigations, ultimately advancing our comprehension of *C. reinhardtii* behavior and its implications for various applications and disciplines.

5.2. Motility & viscosity

Upon comparing the swimming velocity, flagella beating frequency, and viscosity measurement results, it becomes apparent that all three plots exhibit a similar trend from 20 to 40 degrees Celsius. However, it is important to note that these parameters' relationships are not linearly related. A numerical analysis is essential to gain a deeper understanding of how these parameters are linked to each other. We can explore the complex relationships between swimming velocity, flagella beating frequency, and viscosity through numerical anal-

ysis. This analytical approach allows us to quantify the interplay between these factors and identify any potential correlations or dependencies.

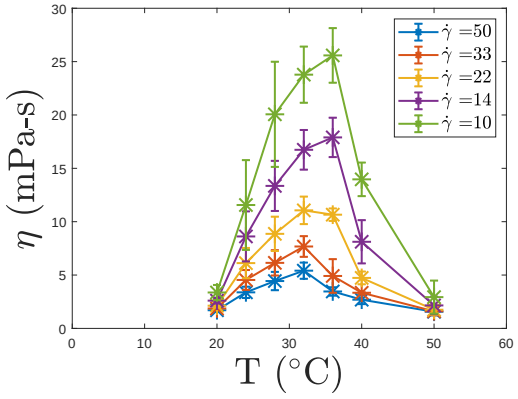

(a) Live cell suspension viscosity at different temperatures and shear rates. Source: Sowmya Kumar. Rheological measurement in our lab.

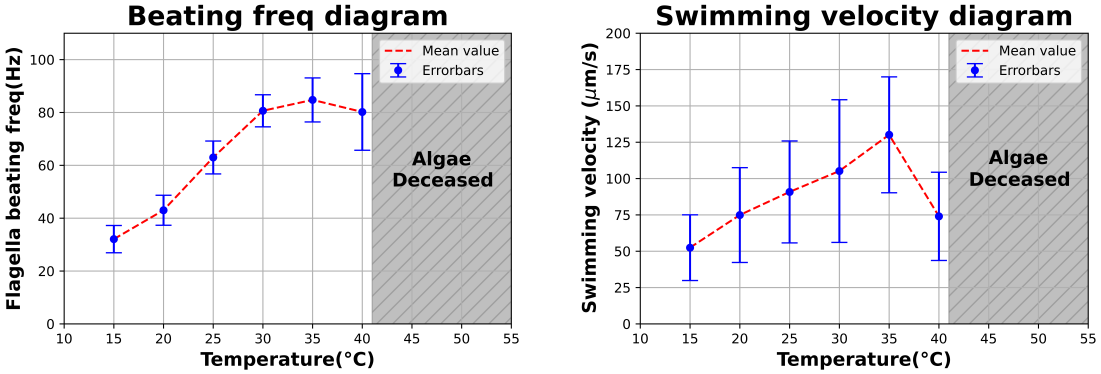

(b) Flagella beating frequency at different temperatures (c) Swimming velocity at different temperatures.

Figure 5.1: Motility and viscosity measurement result comparison.

Live cells' motility plays a crucial role in determining the strength of the stresslet, which refers to a measure of the force and torque exerted by a particle in a fluid medium. In the context of swimming phenomena, such as the beating of flagella, the magnitude of the swimming velocity is closely linked to the magnitude of the stresslet. Equation 2.9 and 2.10 from previous research indicates that higher swimming velocities generally result in an increased force exerted by the beating flagella, leading to an increased stresslet strength.

This relationship can be attributed to the fact that higher swimming velocities cause more rapid changes in the fluid flow patterns generated by the beating motion. As a result, the strength of the stresslet, which characterizes these hydrodynamic interactions, is augmented with increasing swimming velocity. The connection between swimming velocity and stresslet strength is a significant aspect of understanding the dynamic interactions between live cells and their surrounding fluid environment.

In Equation 2.9, the force exerted by live cells is determined by several factors, including the cell's dimensions, the viscosity of the surrounding medium, and the swimming velocity of the cell. Our research has observed variations in swimming velocity and medium viscosity at different temperatures. However, it is important to note that the changes in medium

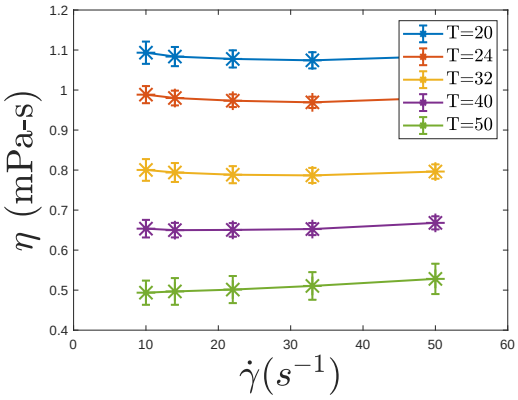

Figure 5.2: TAP medium viscosity results at different temperatures. Source: Sowmya Kumar. Rheological measurement in our lab.

viscosity are not substantial. As shown in Figure 5.2, the viscosity only varies from 1.1 to 0.7mPa·s as the temperature increases from 20 to 40 degrees Celsius. When comparing the variation in live cell swimming velocity with the temperature changes, it is evident that the swimming velocity exhibits significant fluctuations. From 15 to 35 degrees Celsius, the swimming velocity doubles in magnitude, indicating a substantial increase in cell motility over this temperature range. Considering the equation describing the force exerted by live cells, which involves swimming velocity as one of its key factors, the observed doubling of swimming velocity plays a dominant role in determining the force exerted by the cells under different temperatures. While other factors, such as cell dimensions and medium viscosity, also contribute to the force exerted by the cells, the notable change in swimming velocity emerges as the primary driver behind the observed variations in force under different temperature conditions.

The contribution to the bulk stress tensor originating from a volume distribution of such stresslets is expressed as follows [25]:

$$\Sigma^{(s)} = nS(< \mathbf{pp} > -\frac{1}{3}\mathbf{I}) \tag{5.1}$$

The strength of the stresslet created by the live cell is represented by the symbol S, while n (10^{13} cell/m^3) denotes the number of the algae cells per unit volume. Assuming a given shear rate denoted as $\dot{\gamma} = 10s^{-1}$, the calculation of dynamic viscosity at each temperature is straightforward using Equation 5.2.

$$\mu^{(s)} = \frac{\Sigma^{(s)}}{\dot{\gamma}} \tag{5.2}$$

Combining equations 2.9, 2.10, and 5.2 makes it possible to derive a quantitative assessment of viscosity across varying temperatures. As observed in Figure 4, it is evident that the calculated viscosity does not align precisely with our experimental findings. Nonetheless, there is congruence in the trend, with viscosity exhibiting an ascending pattern from 20 to 35 degrees and subsequently declining. The quantitative results, while of a similar order of magnitude (10^{-4}), bear a resemblance to the experimental outcomes (10^{-3}). Notably, our viscosity calculation solely relies on swimming velocity and does not incorporate flagella beating

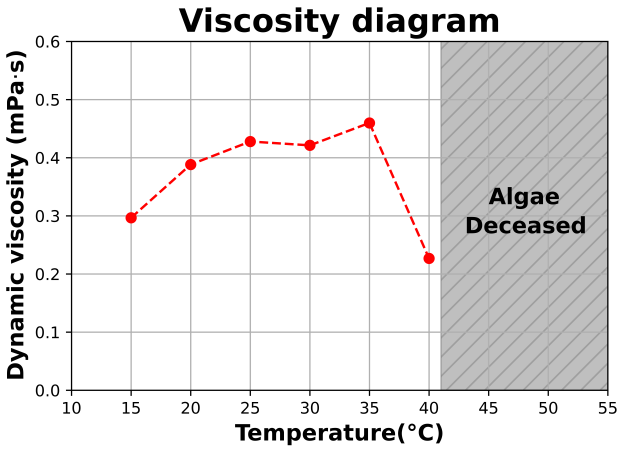

Figure 5.3: Quantitative calculation of dynamic viscosity at different temperatures.

frequency. Furthermore, the stresslet produced by live cells only contributes partially to the overall viscosity. The bulk stress tensor is evaluated by [25]:

$$\Sigma = 2\mu\mathbf{E} + \Sigma^{(\mathrm{p})} + \Sigma^{(\mathrm{d})} + \Sigma^{(\mathrm{s})} \tag{5.3}$$

In Equation 5.3, the symbol $\mathbf{E}$ corresponds to the bulk rate of the strain tensor, while μ represents the viscosity of the suspension. The term $\Sigma^{(\mathrm{p})}$ signifies the stress tensor arising due to the disparity between the deformation and rotation of a suspended cell body compared to the fluid behavior in its absence. Moreover, $\Sigma^{(\mathrm{d})}$ denotes the particle stress emerging from the effective rotational movement of particles, prompted by the rotary diffusion of $\mathbf{p}$ in orientation space. Lastly, $\Sigma^{(\mathrm{s})}$ stands for the stress tensor engendered by the locomotion of live cells.

Therefore, it becomes imperative to conduct additional research on $\Sigma^{(\mathrm{p})}$ and $\Sigma^{(\mathrm{d})}$ across diverse temperature conditions, as this is pivotal for achieving a comprehensive computation of the bulk stress tensor.

5.3. Future work

The motility measurement was conducted in a single experiment involving an increase in temperature from 15 to 40 degrees Celsius without replacing the live cells in the flow cell. However, it is essential to consider that the temperature decrease from 35 to 15 degrees Celsius might have varying impacts on algae behaviors. Further investigations and measurements are warranted to gain a more comprehensive understanding of the effects of temperature variation on algae motility. The measurement interval used in this study was 5 degrees, resulting in a resolution of 5 degrees for temperature data. Exploring a higher resolution, such as a 1 to 2 degrees interval, is recommended to enhance the depth of analysis and insights into live cell motility under different temperatures. This higher-resolution approach can provide valuable knowledge to advance the understanding of the complex relationship between temperature and algae motility. By conducting more experiments and reaching lower temperatures, such as 10 degrees Celsius, researchers can attain a more insightful understanding of the nuances of live cell motility at various temperature conditions.

An alternative approach can be adopted for live algae cells to minimize cell energy loss

during motility measurements under increasing temperature conditions over a relatively long duration. Conducting separate measurements at different temperatures using different flow cells, while using new cells from the same culture group for each temperature, is recommended. This approach ensures that the live cells experience minimal energy loss during the experiments at each specific temperature. By employing this method, the measured swimming velocity and flagella beating frequency at each temperature are expected to be more accurate and reliable. The use of fresh cells and separate flow cells for each temperature eliminates potential variations and disturbances that may arise from prolonged exposure to increasing temperatures. As a result, researchers can obtain more precise data, which enhances the understanding of how temperature affects live algae cell motility.

Swimming velocity and flagella beating frequency are essential aspects of interpreting the motility of live algae cells. However, it is crucial to acknowledge that other relevant parameters, such as helical motion and tumbling frequency, also contribute to the overall motility of the cells. These additional parameters play a significant role in understanding the complete picture of algae motility. To comprehensively investigate the motility of live algae cells, it is imperative to determine and analyze these parameters at each temperature. By studying the relationship between these parameters and the rheological properties of the surrounding medium, researchers can gain valuable insights into the complex interactions between live cells and their fluid environment.

6

Conclusion

Algae play a significant role in our daily life and are closely linked to the environment. The motivation behind this thesis research stems from the need to investigate the rheology of live algae cell suspensions. The motility of live cells under different temperatures can substantially impact the rheological properties, and this aspect has been relatively underexplored in the literature review. The research focuses on interpreting motility through live cell swimming velocity and flagella beating frequency and their correlation with the viscosity of the live suspension.

An experimental setup capable of observing and capturing live cells at different temperatures is essential to achieve this. Temperature control and water circulation are utilized in the study. Both 2D and 3D tracking methods are implemented for motility measurement and analysis. The findings indicate that swimming velocity and beating frequency exhibit a similar increasing trend as the temperature rises from 15 to 35 degrees Celsius, with a peak value observed at 35 degrees, followed by a decrease from 35 to 40 degrees.

The observed motility trend aligns with the viscosity of the live cell suspension measurement, providing evidence that the motility of live cells can indeed affect the rheological properties of the suspension. Previous numerical research has suggested that beating frequency and swimming velocity simultaneously influence the dynamic viscosity of the live suspension, underscoring the importance of investigating the motility of live algae cells under different temperatures.

This study suggests that the motility of live algae cells has multiple ways to interpret and modulate the rheology of the suspension. As such, further investigations into the motility of live algae cells under various temperature conditions are warranted. Exploring the diverse aspects of motility and its implications for rheological properties can significantly contribute to understanding algae behavior and its impact on environmental and industrial applications.

Appendices

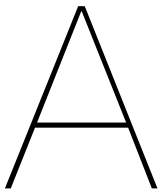

Temperature control code

```
#include <OneWire.h>
#include <DallasTemperature.h>

// Data wire is plugged into digital pin 2 on the Arduino
#define ONE_WIRE_BUS 2

// Setup a oneWire instance to communicate with any OneWire device
OneWire oneWire(ONE_WIRE_BUS);

// Pass oneWire reference to DallasTemperature library
DallasTemperature sensors(&oneWire);

int deviceCount = 0;
float tempC;
float SetTemperature = 40; // Target temperature
float PID_error = 0;
float previous_error = 0;
float elapsedTime, Time, timePrev;
float temp0;
float cumulError;
float myTime = 0;

float PID_value = 0;
//PID constant:
float PID_p = 0; float PID_i = 0; float PID_d = 0;

int motor1pin1 = 4;
int motor1pin2 = 5;

int motor2pin1 = 6;
int motor2pin2 = 7;
//motor 2 is for the Peltier
// 4,5,6,7 are for polarity. 9 and 10 for PWM
```

```
void setup(void)
{
  sensors.begin(); // Start up the library
  Serial.begin(9600);

  // locate devices on the bus
  // Serial.print("Locating devices...");
  // Serial.print("Found ");
  deviceCount = sensors.getDeviceCount();
  // Serial.print(deviceCount, DEC);
  // Serial.println(" devices.");
  // Serial.println("");

   // put your setup code here, to run once:
  pinMode(motor1pin1, OUTPUT);
  pinMode(motor1pin2, OUTPUT);
  pinMode(motor2pin1, OUTPUT);
  pinMode(motor2pin2, OUTPUT);

  pinMode(9, OUTPUT);
  pinMode(10, OUTPUT);
  //pin 10 is for the peltier: heating adjustment

  sensors.requestTemperatures();
  temp0 = sensors.getTempCByIndex(0);
  // Serial.print(temp0);
  // Serial.println("");
}

void loop(void)
{
  // Send command to all the sensors for temperature conversion
  sensors.requestTemperatures();

  // Display temperature from each sensor
  for (int i = 0;  i < deviceCount;  i++)
  {
    // Serial.print("Sensor ");
    // Serial.print(i+1);
    // Serial.print(" : ");
    tempC = sensors.getTempCByIndex(i);
    Serial.print(tempC);
    // Serial.print("C  |  ");
  }

  //For derivative we need real time to calculate speed change rate
  timePrev = Time;                            // the previous time is stored before the actual time read
  Time = millis();                            // actual time read
  elapsedTime = (Time - timePrev) / 1000;     // used to calculate D value

if(SetTemperature >= tempC) // this is for HEATING the peltier element
{//PID VALUES
  int kp = 255; float ki = 1; float kd =20; // change these to constants that work well
  delay(elapsedTime);
```

```
  //Next we calculate the error between the setpoint and the real value
  PID_error = SetTemperature - tempC;
  //Calculate the P value
  PID_p = kp * PID_error;
  //Calculate the I value in a range on +-1
  if(abs(PID_error) <1)
  {
    cumulError +=PID_error*elapsedTime;
    PID_i = ki*cumulError;
  }
  else
  {
    PID_i = 0;
  }

  PID_d = kd*((PID_error - previous_error)/elapsedTime);
  //Final total PID value is the sum of P + I + D
  PID_value = PID_p + PID_i + PID_d;

  //We define PWM range between 0 and 255
  if(PID_value < 0)
  {    PID_value = 0;    }
  if(PID_value > 255)
  {    PID_value = 255;  }

  Serial.print("PWM value =");
  Serial.print(PID_value);
  Serial.print(" Heating  ");
  Serial.print("P = ");
  Serial.print(PID_p);
  Serial.print(" I =");
  Serial.print(PID_i);
  Serial.print(" D = ");
  Serial.print(PID_d);
  Serial.println("");

   // put your main code here, to run repeatedly:

  //Controlling speed (0 = off and 255 = max speed):
  analogWrite(10, PID_value); //ENA pin 255-PID_value provides a PWM signal to pin 10 on the H bridge
  previous_error = PID_error;     //Remember to store the previous error for next loop.
  digitalWrite(motor2pin1, HIGH);
  digitalWrite(motor2pin2, LOW);
}

else//desired temperature is lower than the current temperature
{//PID VALUES
  float kp = 255; float ki_c = 1; float kd =20 ; // change these to constants that work well
  delay(elapsedTime);
  //Next we calculate the error between the setpoint and the real value
  PID_error = tempC - SetTemperature;
  //Calculate the P value
  PID_p = kp * PID_error;
  //Calculate the I value in a range on +-1
```

```
  if(abs(PID_error) <1)
  {
    cumulError +=PID_error*elapsedTime;
    PID_i = ki_c*cumulError;
  }
    else
  {
    PID_i = 0;
  }

  PID_d = kd*((PID_error - previous_error)/elapsedTime);
  //Final total PID value is the sum of P + I + D
  PID_value = PID_p + PID_i + PID_d;

  //We define PWM range between 0 and 255
  if(PID_value < 0)
  {    PID_value = 0;    }
  if(PID_value > 255)
  {    PID_value = 255;  }

  Serial.print("PWM value =");
  Serial.print(PID_value);
  Serial.print("Cooling");
  Serial.print("P = ");
  Serial.print(PID_p);
  Serial.print(" I =");
  Serial.print(PID_i);
  Serial.print(" D = ");
  Serial.print(PID_d);
  Serial.println("");
   // put your main code here, to run repeatedly:

  //Controlling speed (0 = off and 255 = max speed):
  analogWrite(10, PID_value); //ENA pin 255-PID_value provides a PWM signal to pin 10 on the H bridge
  previous_error = PID_error;     //Remember to store the previous error for next loop.
   digitalWrite(motor2pin1, LOW);  //the polarity is reversed --> peltier starts cooling
   digitalWrite(motor2pin2, HIGH);
}

  //controlling speed of pump
  // analogWrite(9, 255); //ENB pin
  // //Controlling spin direction of motors:
  // digitalWrite(motor1pin1, LOW);
  // digitalWrite(motor1pin2, HIGH);
  // Serial.print("Time(s): ");
  myTime = millis(); // acquire the time that how long does the code has been running
  Serial.println(myTime/1000); // prints time since program started

}
```

B

Passive particles velocity

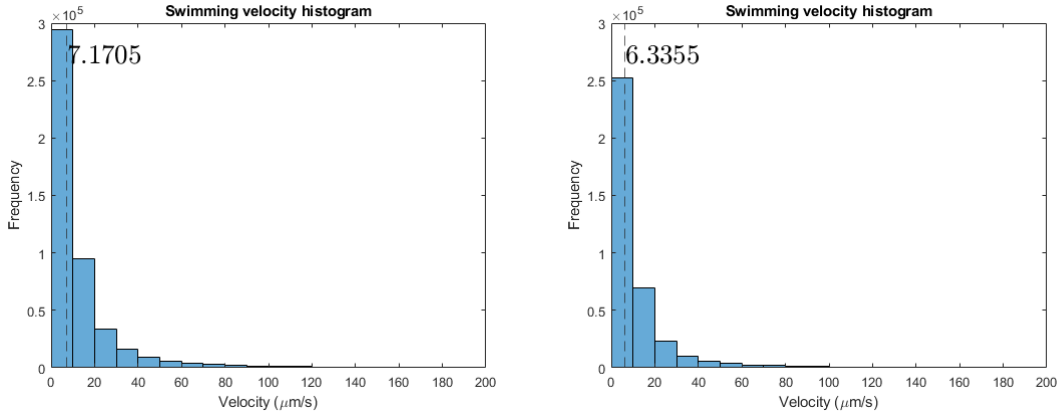

(a) 15 degrees Celsius

(b) 20 degrees Celsius

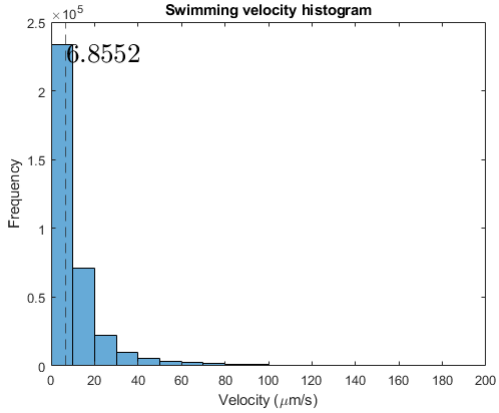

(c) 25 degrees Celsius

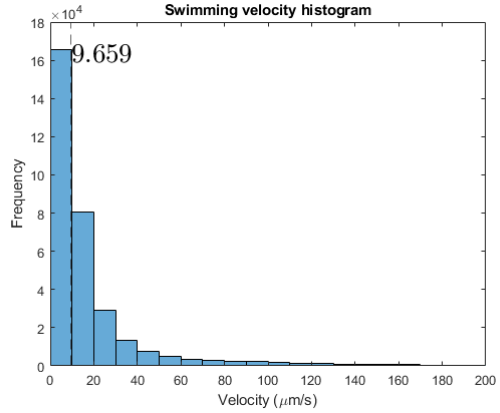

(d) 30 degrees Celsius

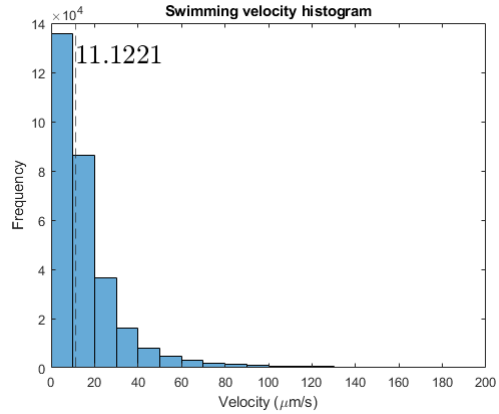

(e) 35 degrees Celsius

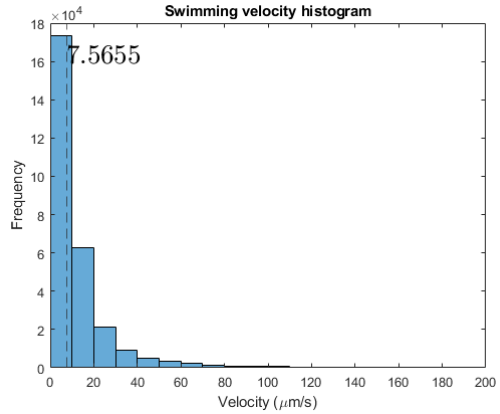

(f) 40 degrees Celsius

Figure B.1: Passive particles velocity distribution at different temperatures. The dashed line represents the median value.

C

Swimming velocity complete data

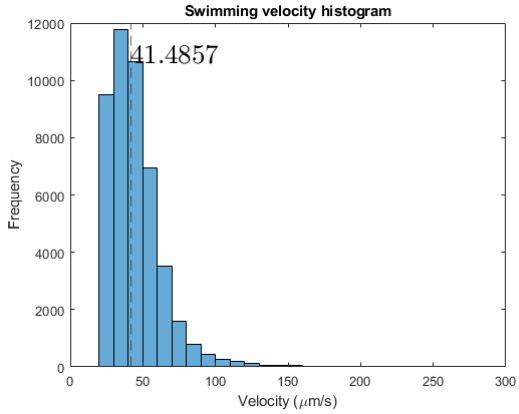

(a) First individual result

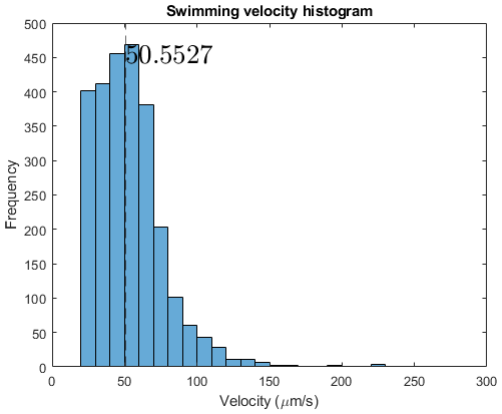

(b) Second individual result

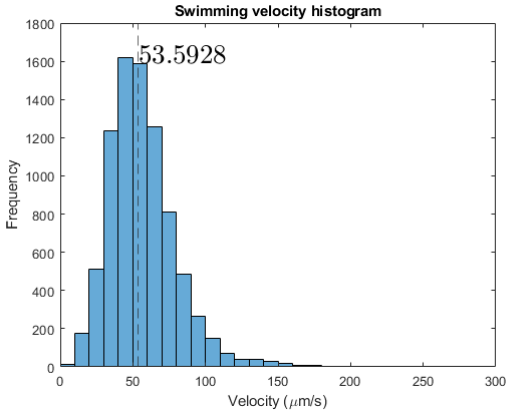

(c) Third individual result

Figure C.1: Swimming velocity results on different days at 15 degrees Celsius.

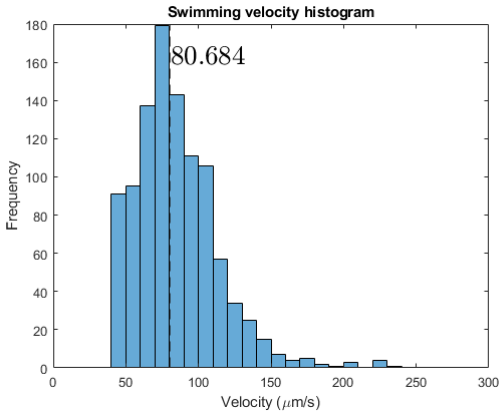

(a) First individual result

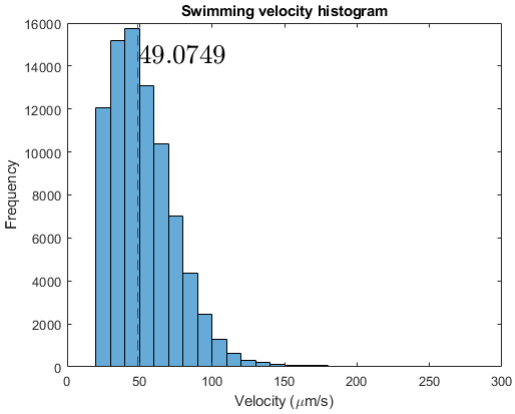

(b) Second individual result

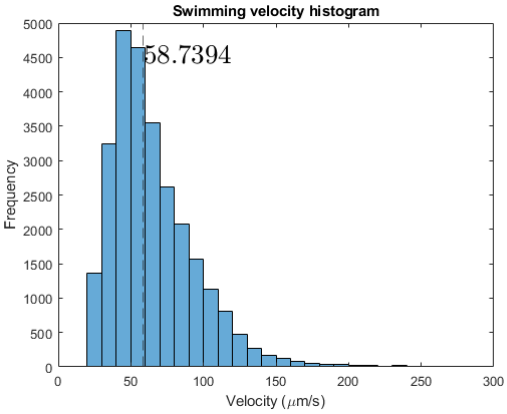

(c) Third individual result

Figure C.2: Swimming velocity results on different days at 20 degrees Celsius.

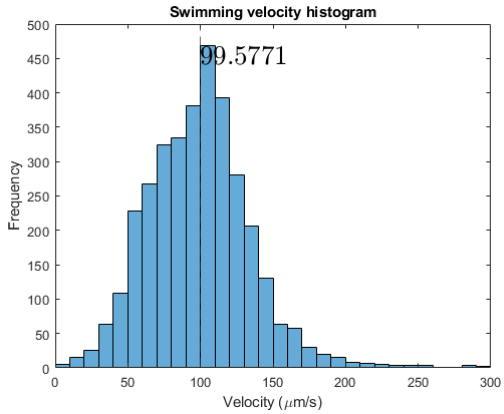

(a) First individual result

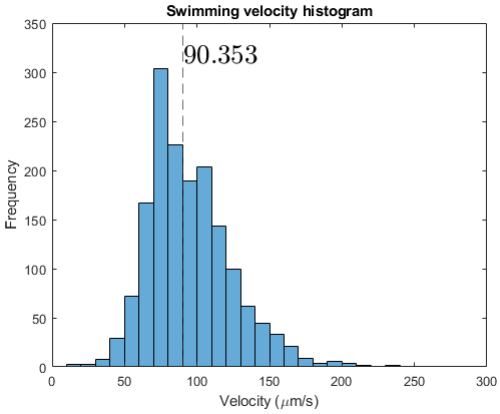

(b) Second individual result

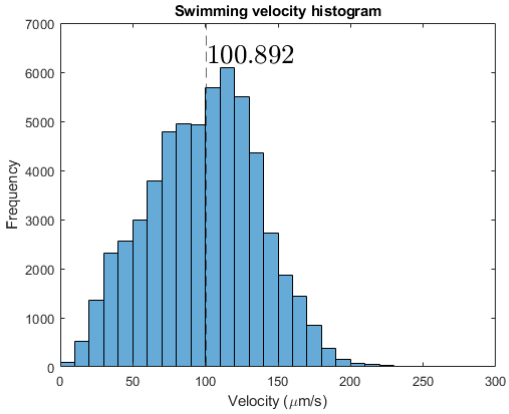

(c) Third individual result

Figure C.3: Swimming velocity results on different days at 25 degrees Celsius.

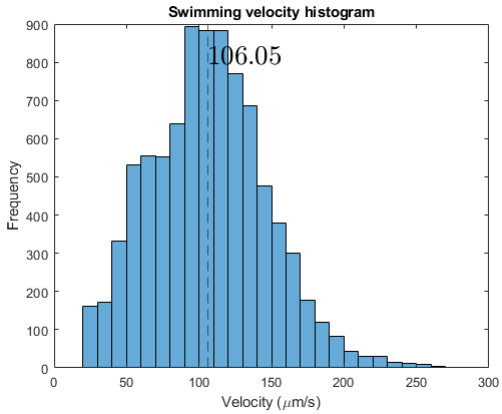

(a) First individual result

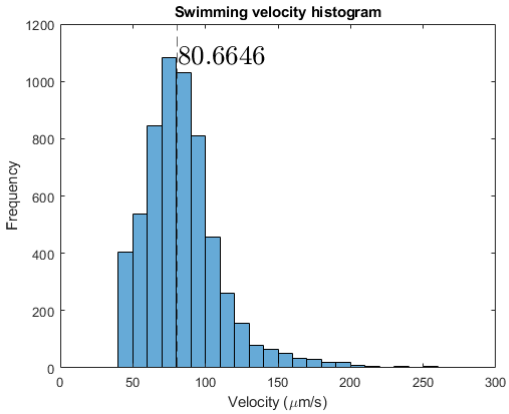

(b) Second individual result

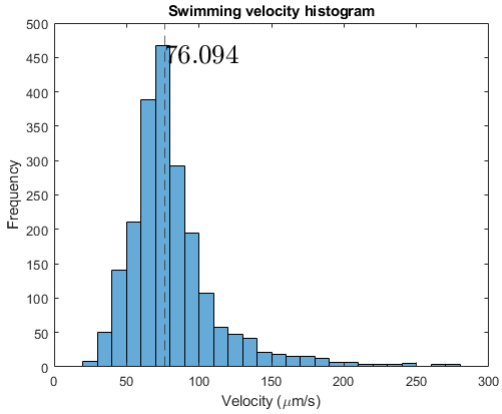

(c) Third individual result

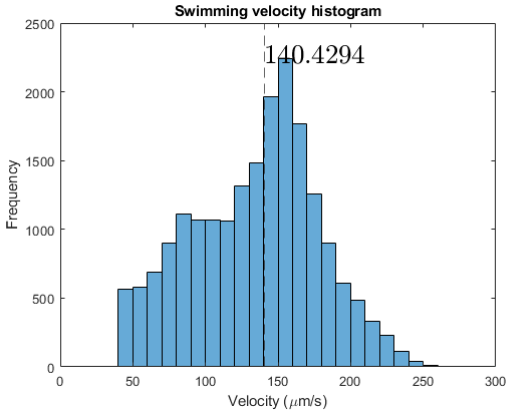

(d) Fourth individual result

Figure C.4: Swimming velocity results on different days at 30 degrees Celsius.

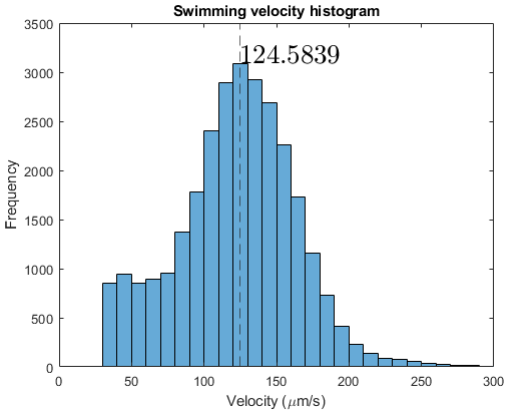

(a) First individual result

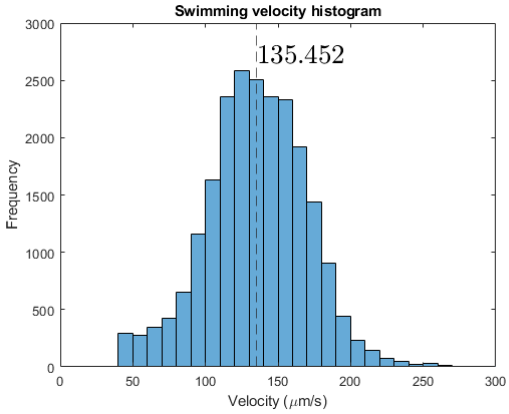

(b) Second individual result

Figure C.5: Swimming velocity results on different days at 35 degrees Celsius.

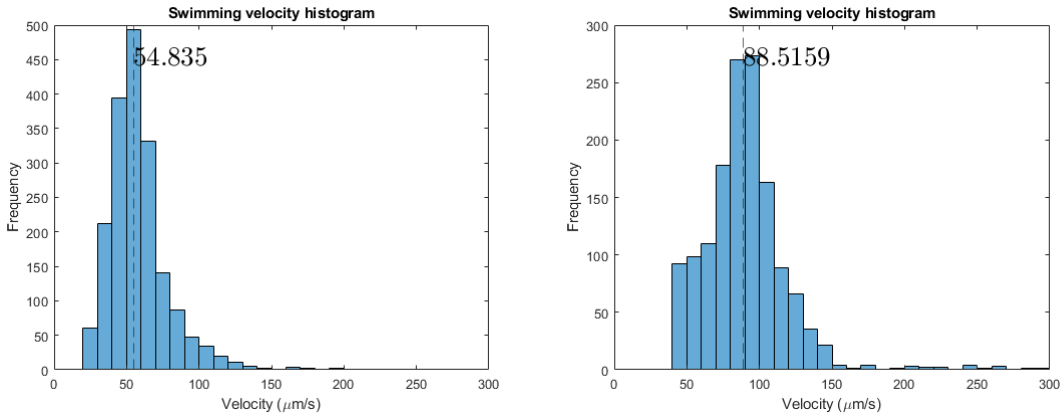

(a) First individual result

(b) Second individual result

Figure C.6: Swimming velocity results on different days at 40 degrees Celsius.

Bibliography

[1] LM Andrade et al. “Chlorella and spirulina microalgae as sources of functional foods”. In: *Nutraceuticals, and Food Supplements* 6.1 (2018), pp. 45–58.

[2] GK Batchelor. “The stress system in a suspension of force-free particles”. In: *Journal of fluid mechanics* 41.3 (1970), pp. 545–570.

[3] JT Bonner. “Evolutionary strategies and developmental constraints in the cellular slime molds”. In: *The American Naturalist* 119.4 (1982), pp. 530–552.

[4] Rajendra P Chhabra. “Non-Newtonian fluids: an introduction”. In: *Rheology of complex fluids* (2010), pp. 3–34.

[5] Walter K Dodds, Dolly A Gudder, and Dieter Mollenhauer. “The ecology of Nostoc”. In: *Journal of Phycology* 31.1 (1995), pp. 2–18.

[6] Matthew T Downton and Holger Stark. “Simulation of a model microswimmer”. In: *Journal of Physics: Condensed Matter* 21.20 (2009), p. 204101.

[7] Kunshan Gao. “Chinese studies on the edible blue-green alga, Nostoc flagelliforme: a review”. In: *Journal of Applied Phycology* 10 (1998), pp. 37–49.

[8] Christoph Griesbeck, Iris Kobl, and Markus Heitzer. “Chlamydomonas reinhardtii”. In: *Molecular biotechnology* 34.2 (2006), pp. 213–223.

[9] Hans-Peter Grossart, Lasse Riemann, and Farooq Azam. “Bacterial motility in the sea and its ecological implications”. In: *Aquatic Microbial Ecology* 25.3 (2001), pp. 247–258.

[10] Gustaaf M Hallegraeff. “Ocean climate change, phytoplankton community responses, and harmful algal blooms: a formidable predictive challenge 1”. In: *Journal of phycology* 46.2 (2010), pp. 220–235.

[11] Elizabeth H Harris. “Chlamydomonas as a model organism”. In: *Annual review of plant biology* 52.1 (2001), pp. 363–406.

[12] Yashodhan Hatwalne et al. “Dynamics and Rheology of Active-Particle Suspensions”. In: *APS March Meeting Abstracts*. Vol. 2004. 2004, pp. L9–012.

[13] A.J.K. Heijdra et al. *Design of a temperature-controlled Microbioreactor for tracking swimming velocity of microalgae cells*. Delft University of Technology, 2022.

[14] Ritsu Kamiya and Etsuko Hasegawa. “Intrinsic difference in beat frequency between the two flagella of Chlamydomonas reinhardtii”. In: *Experimental cell research* 173.1 (1987), pp. 299–304.

[15] Ioannis Karatzas et al. “Brownian motion”. In: *Brownian motion and stochastic calculus* (1998), pp. 47–127.

[16] *LaVision*. `https://www.lavision.de/en/products/cameras/cameras-for-piv/`. Accessed: 2023-07-03.

[17] Gao-Jin Li and Arezoo M Ardekani. “Hydrodynamic interaction of microswimmers near a wall”. In: *Physical Review E* 90.1 (2014), p. 013010.

[18] Héctor Matías López et al. “Turning bacteria suspensions into superfluids”. In: *Physical review letters* 115.2 (2015), p. 028301.

[19] TOSHIKAZU MAJIMA and FUMIO OOSAWA. “Response of Chlamydomonas to temperature change”. In: *The Journal of Protozoology* 22.4 (1975), pp. 499–501.

[20] K. Muller. “Collective Swimming Dynamics of Motile Micro-Algae: Cell-Wall and Cell-Cell Interactions”. MA thesis. Delft University of Technology, 2016.

[21] Takuji Narumi et al. “Thermotaxis”. In: *SIGGRAPH'09: Posters*. 2009, pp. 1–1.

[22] *New bioreactor to speed production of microalgae for feed, fuel uses*. https://www.feednavigator.com/Article/2017/08/11/New-bioreactor-to-speed-production-of-microalgae-for-feed-fuel-uses. Accessed: 2023-06-03.

[23] *Nikon Instruments Inc.* https://www.microscope.healthcare.nikon.com/products/inverted-microscopes/eclipse-ti2-series. Accessed: 2023-07-01.

[24] K.A. van Overhagen. “Designing Rheology tools for active and complex fluids”. MA thesis. Delft University of Technology, 2022.

[25] TJ Pedley and John O Kessler. “A new continuum model for suspensions of gyrotactic micro-organisms”. In: *Journal of fluid mechanics* 212 (1990), pp. 155–182.

[26] Salima Rafaï, Levan Jibuti, and Philippe Peyla. “Effective viscosity of microswimmer suspensions”. In: *Physical Review Letters* 104.9 (2010), p. 098102.

[27] Carl Safi et al. “Morphology, composition, production, processing and applications of Chlorella vulgaris: A review”. In: *Renewable and Sustainable Energy Reviews* 35 (2014), pp. 265–278.

[28] David Saintillan. “Rheology of active fluids”. In: *Annual Review of Fluid Mechanics* 50 (2018), pp. 563–592.

[29] Martha Sanchez et al. “Spirulina (Arthrospira): an edible microorganism: a review”. In: *Universitas Scientiarum* 8.1 (2003), pp. 7–24.

[30] Masaya Sekiguchi et al. “Thermotaxis Involves Spontaneous Backward Swimming in Chlamydomonas”. In: *Biophysical Journal* 116.3 (2019), 548a.

[31] Ajay Vikram Singh et al. “Mechanical coupling of puller and pusher active microswimmers influences motility”. In: *Langmuir* 36.19 (2020), pp. 5435–5443.

[32] Saverio E Spagnolie and Eric Lauga. “Hydrodynamics of self-propulsion near a boundary: predictions and accuracy of far-field approximations”. In: *Journal of Fluid Mechanics* 700 (2012), pp. 105–147.

[33] Pauline Spolaore et al. “Commercial applications of microalgae”. In: *Journal of bioscience and bioengineering* 101.2 (2006), pp. 87–96.

[34] *Squeeze water filtration system*. URL: https://www.sawyer.com/products/squeeze-water-filtration-system.

[35] Daisuke Takagi and J Rudi Strickler. “Active hydrodynamic imaging of a rigid spherical particle”. In: *Scientific Reports* 10.1 (2020), pp. 1–10.

[36] Tetsuo Takahashi and Masakatsu Watanabe. “Photosynthesis modulates the sign of phototaxis of wild-type Chlamydomonas reinhardtii: Effects of red background illumination and 3-(3’, 4’-dichlorophenyl)-1, 1-dimethylurea”. In: *FEBS letters* 336.3 (1993), pp. 516–520.

[37] Roger I Tanner. *Engineering rheology*. Vol. 52. OUP Oxford, 2000.

[38] Roger I Tanner and Kenneth Walters. *Rheology: an historical perspective*. Vol. 7. Elsevier, 1998.

[39] Da Wei et al. “Is the zero Reynolds number approximation valid for ciliary flows?” In: *Physical review letters* 122.12 (2019), p. 124502.

[40] Wikipedia contributors. *Non-Newtonian fluid — Wikipedia, The Free Encyclopedia*. [Online; accessed 26-January-2023]. 2023. URL: `https://en.wikipedia.org/w/index.php?title=Non-Newtonian_fluid&oldid=1134875651`.